

UC Merced

UC Merced Electronic Theses and Dissertations

Title

Synthesis and Crystallization of Tetraanilines as New Organic Electronic Materials

Permalink

<https://escholarship.org/uc/item/7fw8d0tt>

Author

Fadamin, Arghavan

Publication Date

2020

Peer reviewed|Thesis/dissertation

UNIVERSITY OF CALIFORNIA MERCED

Synthesis and Crystallization of Tetraanilines as New Organic Electronic
Materials

A Thesis submitted in partial satisfaction of the requirements
for the degree of Master of Science

in

Chemistry and Chemical Biology

by

Arghavan Fadamin

Committee in charge:

Professor Ryan Baxter, Chair

Professor Christopher Viney

Professor Tao Ye

Professor Yue (Jessica) Wang, Advisor

© Arghavan Fadamin, 2020
All Rights Reserved

The Thesis of Arghavan Fadamin is approved, and it is accepted
in quality and form for publication on microfilm and electronically:

Professor Ryan Baxter, Chair

Professor Christopher Viney

Professor Tao Ye

Professor Yue (Jessica) Wang, Advisor

University of California, Merced

2020

TABLE OF CONTENTS

SIGNATURE PAGE	iii
TABLE OF CONTENTS	iv
LIST OF ABBREVIATIONS	vii
LIST OF FIGURES	xi
LIST OF SCHEMES	xiii
LIST OF TABLES	xiv
ACKNOWLEDGMENTS	xv
ABSTRACT	xvi
CHAPTER I. Background	
I.1 Introduction.....	1
I.2 An oligomer approach.....	3
I.3 The oxidation-reduction chemistry of polyaniline.....	3
I.4 Charge transport properties in conducting polymers.....	5
References.....	8
CHAPTER II. Synthesis of TANI oligomers	
II.1 The abbreviation of all TANI oligomers used in this study.....	9
II.2 Synthetic routes for making Ph/Ph TANI in LE oxidation state.....	10
II.3 Buchwald-Hartwig cross-coupling reaction.....	13
II.3.1 Catalytic cycle.....	14
II.4 The oxidation of TANI LE to EB state.....	15
II.5 Synthetic procedures for various Ph/Ph end-capped TANI.....	16
II.5.1 Preparation of compound 1LE.....	16

II.5.2 Preparation of compound 2LE.....	17
II.5.3 Preparation of compound 3LE.....	18
II.5.4 Preparation of compound 4LE.....	19
II.5.5 Preparation of compound 5LE.....	19
II.5.6 Preparation of compound 6LE.....	20
II.5.7 Preparation of compound 1EB.....	21
II.5.8 Preparation of compound 2EB.....	21
II.5.9 Preparation of compound 3EB.....	22
References.....	23

CHAPTER III. Characterization of TANI oligomers

III.1 ¹ H-NMR spectroscopy.....	24
III.1.1 Characterization of compound 1LE.....	24
III.1.2 Characterization of compound 2LE.....	25
III.1.3 Characterization of compound 3LE.....	25
III.1.4 Characterization of compound 4LE.....	26
III.1.5 Characterization of compound 5LE.....	27
III.1.6 Characterization of compound 6LE.....	28
III.1.7 Characterization of compound 1EB.....	28
III.1.8 Characterization of compound 2EB.....	29
III.1.9 Characterization of compound 3EB.....	30
III.2 UV-vis spectroscopy.....	31
References.....	35

CHAPTER IV. Crystallization

IV.1 Nucleation.....36

IV.2 Homogenous and heterogeneous nucleation.....39

IV.3 Classical nucleation theory (CNT)40

IV.4 Two-step nucleation theory.....41

IV.5 The morphology and growth of crystals.....42

IV.5.1 Wulff construction of surface energy.....42

IV.6 Growth kinetics.....43

IV.7 Different techniques for growing single crystal.....45

IV.8 Vapor diffusion results.....46

IV.9 Layering results.....47

Reference.....49

CHAPTER. Conclusion.....51

LIST OF ABBREVIATIONS

This list is in alphabetical order.

1D	1-Dimensional
1EB	4,4'-(((1E,4E)-cyclohexa-2,5-diene-1,4-diylidene)-bis(azaneylylide)-bis(N-phenylaniline))
1LE	N ¹ , N ^{1'} -(1,4-phenylene)-bis(N ⁴ -phenylbenzene-1,4-diamine)
2D	2-Dimensional
2EB	4,4'-(((1E,4E,4'E)-[1,1'-bi(cyclohexylidene)]-2,2',5,5'-tetraenylidene-4,4'-diylidene)-bis(azaneylylidene))-bis(N-phenylaniline)
2LE	N ¹ , N ^{1'} -(biphenyl-4,4'-diyl)-bis(N ⁴ -phenylbenzene-1,4-diamine)
3EB	4,4'-(((2E,6E)-naphthalene-2,6-diylidene)-bis(azaneylylidene))-bis(N-phenylaniline)
3LE	N ¹ , N ^{1'} -(naphthalene-2,6-diyl)-bis(N ⁴ -phenylbenzene-1,4-diamine)
4EB	N ¹ , N ^{1'} -(naphthalene-1,4-diylidene)-bis(azaneylylidene)-bis(N-phenylaniline)
4LE	N ¹ , N ^{1'} -(naphthalene-1,4-diyl)-bis(N ⁴ -phenylbenzene-1,4-diamine)
5EB	4,4'-(((1E,4E)-2,5-dimethylcyclohexa-2,5-diene-1,4-diylidene)-bis(azaneylylidene))-bis(N-phenylaniline)
5LE	N ¹ , N ^{1'} -(2,5-dimethyl-1,4-phenylene)-bis(N ⁴ -phenylbenzene-1,4-diamine)
6EB	4,4'-(((1E,4E)-2,5-dimethoxycyclohexa-2,5-diene-1,4-diylidene)-bis(azaneylylidene))-bis(N-phenylaniline)
6LE	N ¹ , N ^{1'} -(2,5-dimethoxy-1,4-phenylene)-bis(N ⁴ -phenylbenzene-1,4-diamine)
α	Alpha
Abbr	Abbreviation
APS	Ammonium persulfate

aq	Aqueous
β	Beta
BINAP	(2,2'-bis(diphenylphosphino)-1,1'-binaphthyl)
$^{\circ}\text{C}$	Celsius
C-N	Carbon-nitrogen bond
CNT	Classical nucleation theory
dba	Dibenzylideneacetone
DMF	Dimethylformamide
DMSO	Dimethyl sulfoxide
EB	Emeraldine base
eq	Molar equivalent
ES	Emeraldine salt
HOMO	Highest occupied molecular orbital
I-V	Current-voltage
λ	Lambda
LE	Lucoemeraldine
LUMO	Lowest unoccupied molecular orbital
M	Molar
MALDI	Matrix-assisted laser desorption/ionization
max	Maximum
mg	Milligram
MHz	Megahertz
min	Minute

ml	Milliliter
μm	Micrometer
mm	Millimeter
mmol	Millimole
MPa	Megapascal
MS	Mass spectrometry
n	Nonbonding electrons
nm	Nanometer
NMP	N-methyl-2-pyrrolidone
NMR	Nuclear magnetic resonance
π	Pi
PANI	Polyaniline
Pd	Palladium
Ph	Phenyl
ppm	Part per million
r	Radius
rac	Racemic
S.cm ⁻¹	Siemens per centimeter
SEM	Scanning electron microscope
T	Time
TANI	Tetraaniline
TD-DFT	Time-dependent density functional theory
THF	Tetrahydrofuran

TLC Thin-layer chromatography

TOF Time of flight mass

UV-vis Ultraviolet-visible

LIST OF FIGURES

Figure 1. Conducting polymers applications.....	xvi
Figure 2. Wide-angle X-ray scattering from α -keratin and β -keratin.....	1
Figure 3. Schematic illustration of α -keratin and β -keratin.....	2
Figure 4. The oxidation-reduction chemistry of PANI.....	4
Figure 5. Proposed mechanism of aniline oxidation and PANI formation.....	5
Figure 6. Typical π - π edge-on packing for classic semicrystalline polymers.....	6
Figure 7. Single TANI nanowire on a Si substrate.....	7
Figure 8. $^1\text{H-NMR}$ spectrum of 1LE compound.....	24
Figure 9. $^1\text{H-NMR}$ spectrum of 2LE compound.....	25
Figure 10. $^1\text{H-NMR}$ spectrum of 3LE compound.....	26
Figure 11. $^1\text{H-NMR}$ spectrum of 4LE compound.....	27
Figure 12. $^1\text{H-NMR}$ spectrum of 5LE compound.....	27
Figure 13. $^1\text{H-NMR}$ spectrum of 6LE compound.....	28
Figure 14. $^1\text{H-NMR}$ spectrum of 1EB compound.....	29
Figure 15. $^1\text{H-NMR}$ spectrum of 2EB compound.....	30
Figure 16. $^1\text{H-NMR}$ spectrum of 3EB compound.....	30
Figure 17. UV-vis spectra of leucoemeraldine compounds (1-3).....	31
Figure 18. Generation of second absorption peak upon oxidation.....	32
Figure 19. UV-vis spectra of TANI-EB compounds (1-6).....	34
Figure 20. Free energy change diagram of forming nucleation.....	36
Figure 21. The heterogeneous nucleation.....	40
Figure 22. Schematic illustration for CNT.....	41

Figure 23. Schematic representation of nucleation theories.....	42
Figure 24. Wulff plot scheme.....	43
Figure 25. The face profile in Kossel's model.....	44
Figure 26. A typical liquid-liquid diffusion setup used in growing crystal.....	45
Figure 27. A typical vapor diffusion setup used in growing crystal.....	46
Figure 28. Single crystals of various TANI in the EB oxidation state.....	47
Figure 29. Different solvent used for a single crystal of 4EB and 6EB.....	48

LIST OF SCHEMES

Scheme 1. Summary of Ph/Ph end-caped TANI-LE synthesis of Honzl.....	10
Scheme 2. Summary of Ochi synthesis of Ph/Ph end-caped TANI-LE.....	11
Scheme 3. Summary of Rebourt synthesis of Ph/Ph end-caped TANILE.....	11
Scheme 4. Summary of Gao synthesis of Ph/Ph end-caped TANILE.....	12
Scheme 5. Summary of MacDiarmid synthesis of Ph/Ph end-caped TANILE...	12
Scheme 6. Summary of Kaczorowski synthesis of Ph/Ph end-caped TANILE...	13
Scheme 7. Summary of Faul synthesis of Ph/Ph end-caped TANILE.....	13
Scheme 8. Palladium-catalyzed coupling reaction for oligoaniline Synthesis....	14
Scheme 9. Catalytic cycle for Buchwald-Hartwig coupling.....	15
Scheme 10. Possible positional isomers for Ph/Ph end-caped TANI oligomer...	16
Scheme 11. Summary of the Ph/Ph end-caped TANI-EB synthesis.....	16
Scheme 12. Summary of the 1LE synthesis.....	17
Scheme 13. Summary of the 2LE synthesis.....	18
Scheme 14. Summary of the 3LE synthesis.....	18
Scheme 15. Summary of the 4LE synthesis.....	19
Scheme 16. Summary of the 5LE synthesis.....	20
Scheme 17. Summary of the 6LE synthesis.....	21
Scheme 18. Summary of the 1EB synthesis.....	21
Scheme 19. Summary of the 2EB synthesis.....	22
Scheme 20. Summary of the 3EB synthesis.....	22

LIST OF TABLES

Table 1. Summary of molecular structures and abbreviations of compounds.....	9
Table 2. The maximum absorption wavelength for LE compounds (1-3).....	32
Table 3. The maximum absorption wavelength for EB compounds (1-6).....	33
Table 4. Comparison between λ_{\max} values.....	34

ACKNOWLEDGMENTS

I would like to express gratitude to my advisor, Dr. Yue (Jessica) Wang, because of her supports in my professional and personal life in the past two years. From a professional standpoint, her guidance and experience have always been an enormous advantage that showed me the path wherein sometimes I felt lost in my research or writing. Her supportive attitude regarding the tough decision to master out of the Ph.D. program because of personal matters was a huge help in lifting a heavy weight off my shoulder.

I would like to thank my committee members, Professors Ryan Baxter, Christopher Viney, and Tao Ye for providing valued feedback during my first-year review.

I would like to thank all the members of Wang Lab especially Robert Jordan who was always available to provide guidance and share his experience with me. I feel also highly thankful to my lab mates Kiana, Celeste, Jacob, Ian, Victor, Bohao, John, Miguel, Adrian, by providing the best lab environment.

I also wish to thank the UC Merced chemistry and chemical biology faculties, administrative support, research support staff. And finally, I like to thank my parents and my husband for their endless support and encouragement.

ABSTRACT

Recent advances in the field of organic electronic devices such as supercapacitors, chemical sensors, and field-effect transistors, have brought tremendous attention to conjugated materials. The benefits of these conjugated materials are their significantly lower fabrication cost, low-temperature processing, solution processability, mechanical flexibility, and tunable optoelectronic properties compared to their inorganic counterparts. Figure 1 shows the applications of conducting polymers in electronic devices.

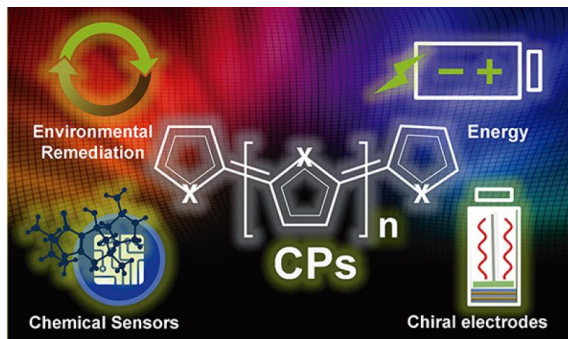


Figure 1. Conducting polymers applications.¹

Among the family of conducting polymers, polyaniline is of particular interest as a result of its ambient stability, distinctive oxidation-reduction chemistry, and the straightforward acid-base doping-dedoping process. However, its properties such as polydispersity, poor processability, complex chain conformation, and poor solubility proved to be challenging for fundamental studies.

The functionality and efficiency of organic electronic devices are dictated by the assembly of polymer chains in the solid-state. The lack of ordered extended structure at the chain level has restricted the incorporation of polyaniline nanostructures such as nanofibers in electronic devices requiring high carrier mobility, which is an essential feature for satisfactory device performance. These applications are currently dominated by molecular semiconductors that can often self-assemble into highly ordered nanowires or nanoribbons.

Oligomers can be considered an intermediate between polymer and molecular semiconductors. Since oligomers are essentially a small section of the parent polymer comprising only a few repeating units, they possess similar chemical properties as the parent polymer. However, in terms of crystallinity and assembly, oligomers resemble molecular semiconductors as they can be synthesized as monodispersed entities and directed to self-assemble into well-ordered crystals and supramolecular morphologies.

One important characteristic of oligomers of aniline is that they are capable of forming ordered extended structures that are not possible with polyaniline. This notable feature in oligomers of aniline provides an opportunity for using them as model systems for exploring the complexity of molecular interactions in polyaniline more in-depth.

In this thesis, oligomers of aniline are chosen as the oligomers of interest to serve as single crystalline model systems for their polymeric analog for the investigation of the intrinsic structure-property relationships in polymers. This knowledge is essential for the application of conducting polymers in the future in various electronic devices.² Specifically, my thesis research focuses on the synthesis, characterization, and crystallization of tetraaniline oligomers. We conducted reaction studies by ¹H-NMR and UV-vis spectroscopy to elucidate the factors affecting reaction pathways. Chapter I provides the background of the field. Chapter II discusses the synthesis of tetraaniline oligomers. Various forms of characterization are covered in Chapter III. The crystallization of these compounds is described in Chapter IV. Finally, conclusions are drawn from this research and future works are described in Chapter V.

CHAPTER I. Background

I.1. Introduction

The recent development in conjugated polymers has enabled a myriad of new applications such as low-cost, flexible solar cells and organic light-emitting diodes.¹ With the rise of next-generation soft electronics and robotics, one major challenge the field has yet to solve is how to create desirable mechanical properties such as low stiffness and high extensibility in conjugated polymers without compromising their electrical properties.² Existing methods rely heavily on complex, multi-step chemical modifications,² which are often not scalable and drive up the cost of these supposedly low-cost materials. One possible solution to this challenge is looking to nature for inspiration.

Nature is an ingenious material scientist. It has developed exceedingly efficient routes towards multi-functional materials with intriguing combinations of properties. Numerous materials with drastically different mechanical properties can be achieved through the hierarchical assembly of the same few chemical building blocks, which are virtually unthinkable in synthetic materials. For example, keratin is a structural biopolymer that serves as the main component in wool, fingernail, hair, hoof, horn, claws, beak, and feather epithelial cells.³ Those materials diverge significantly in mechanical properties but are similar in chemical composition. The secret to such divergence lies in the supramolecular structures of the keratinous material and their hierarchical assembly.

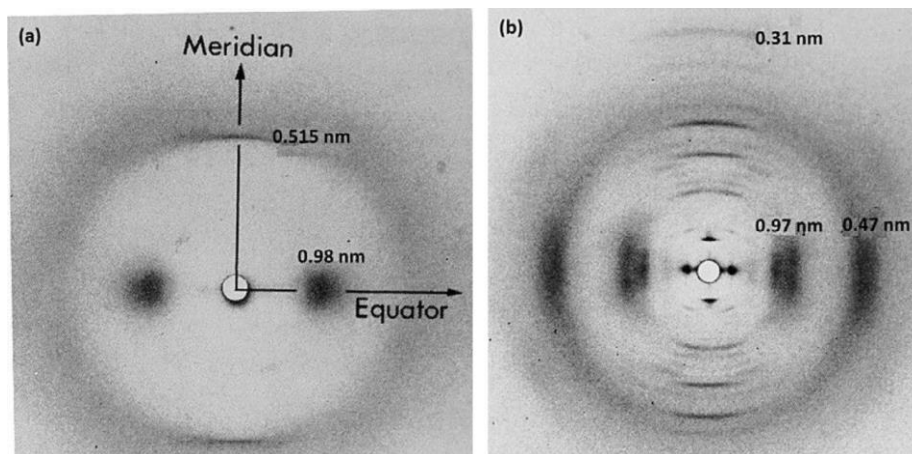


Figure 2. Wide-angle X-ray scattering from (a) α -keratin and (b) β -keratin.³

X-ray diffraction studies have established that keratins can be divided into four distinct patterns: an α -pattern, β -pattern, feather, and amorphous pattern (Figure 2)³. It is well accepted that the feather pattern has a similar helical array of twisted β -pattern.⁴ The key characteristics that distinguish α -keratin from β -

keratin are the variations in their supramolecular structures. Both α - and β -keratinous materials show a fine nanoscale filament matrix. α -keratin has essentially coiled-coil structure and forms 1D fibers. The α helical fibers are flexible, elastic, and can be extended twice of their length. On the other hand, β -keratin filaments instead consist of 2D sheet structures and are rigid, not stretchable, and provide strength (Figure 3).³ As a result, biological materials can have drastically different mechanical properties depending on whether α -keratin or β -keratin is the filler material embedded in the amorphous keratin matrix, even though they essentially have the same chemical composition.

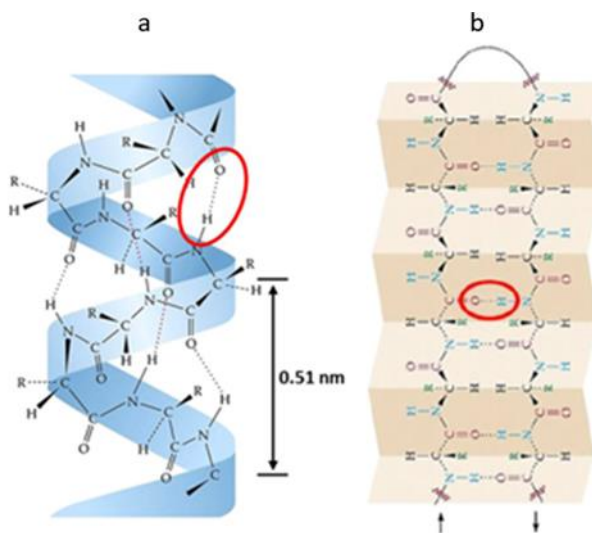


Figure 3. Schematic illustration of (a) α -keratin (b) β -keratin.³

The fiber orientation can also make a big difference in material properties. For example, human hair exhibits tensile strength of 150-270 MPa^{3a} as a result of the high orders of alignment of α -helices along its length. On the other hand, human nail tensile strength is 5 times lower^{3b} because the α -helices inside have less alignment. Essentially, even with the same chemical composition (keratin) and the same crystalline keratin fiber-to-amorphous keratin matrix ratio, we can control the mechanical properties of the composites just by changing fiber orientation.

With this knowledge in mind, we mimic these design principles found in biological systems and apply them to tune the mechanical and possibly other physical properties of conjugated polymers without changing their chemical composition or mixing foreign substances. In other words, we envision to create disordered and ordered phases separately using the same material, and combine them in a controlled, hierarchical fashion to access a wide range of mechanical properties while preserving their electrical properties. This powerful approach

allows us to stop synthesizing new polymers for every new, desirable functionality, but to conceive them through existing chemical building blocks, which is more environmentally friendly and sustainable.

A disordered phase and an ordered phase are needed for creating such bio-inspired composites. My thesis research specifically focuses on the synthesis, characterization, and crystallization of tetraanilines as potential single crystalline, conductive filler materials for their disordered parent polymer matrices. Both phases will share the same chemical composition, much like the keratinous materials described above. In addition to the allure of using the oligomer crystals for creating bioinspired compositionally homogenous composites, these crystals can be used as model systems for investigating intrinsic structure-property relationships in parent polymer such as the effect of molecular structures on (1) crystallographic packing, (2) electrical properties, and (3) mechanical properties, which can provide valuable fundamental insights.

I.2. An oligomer approach

The subject of conducting polymers, particularly polyaniline (PANI) has undergone a variety of advances from the first reported paper on PANI preparation by the electrolysis of sulfate of aniline following by subsequent studies on various oxidation states^{5,6} and was greatly extended by studies of Shirakawa and MacDiarmid which led to a Nobel prize in 2000.

One of the major drawbacks of π -conjugated polymers (i.e. PANI) is their poor solubility and processability which limits their application in low-temperature solution-processed electronic devices. In contrast to polymers, oligomers are great model systems of their parent polymers as they are free from grain boundaries or molecular disorder. Studying them at the molecular level allows us to broaden our fundamental knowledge about polymers. Therefore, we need to synthesize monodispersed oligomer molecules, fully characterize them, and crystallize them into single-crystalline entities.

I.3. The oxidation-reduction chemistry of polyaniline (PANI)

The difference in benzenoid-to-quinoid ratio generates different oxidation states for PANI; (1) the fully reduced leucoemeraldine state possesses four benzene rings and no quinoid ring in its repeating structure; (2) the fully oxidized pernigraniline state possesses two benzene rings and two quinoid rings in its repeating structure; (3) half oxidized and half reduced emeraldine base (EB) form possesses three benzene rings and one quinoid ring in its repeating structure and is the most important oxidation state. EB can be doped reversibly by strong acid ($\text{pH} < 2.5$) to form the conductive emeraldine salt (ES) form and have conductivity $>1 \text{ S}\cdot\text{cm}^{-1}$. The dedoping process by adding a strong base can yield

the insulating EB state with conductivity $\leq 1 \times 10^{-10} \text{ S}\cdot\text{cm}^{-1}$.⁷ Figure 4 indicates the oxidation-reduction chemistry of PANI.⁸

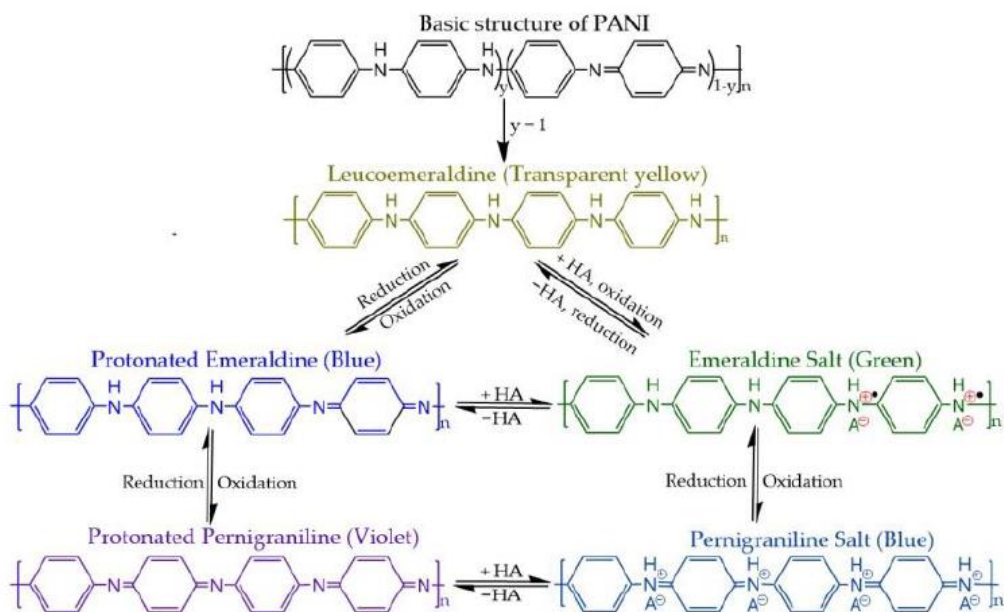


Figure 4. The oxidation-reduction chemistry of PANI.⁸

PANI can be generated by chemical polymerization using an oxidizing agent or electrochemical methods using a suitable voltage. The oxidation of aniline produces radical cation in the initiation step. This radical cation species can react with another radical molecule through the para position to produce dimer or trimer. The chains grow as additional aniline monomer radicals are added to the active chain ends. It is believed that the reoxidation of terminal radical cation species results in the termination step.⁹ The proposed mechanism is illustrated in Figure 5.

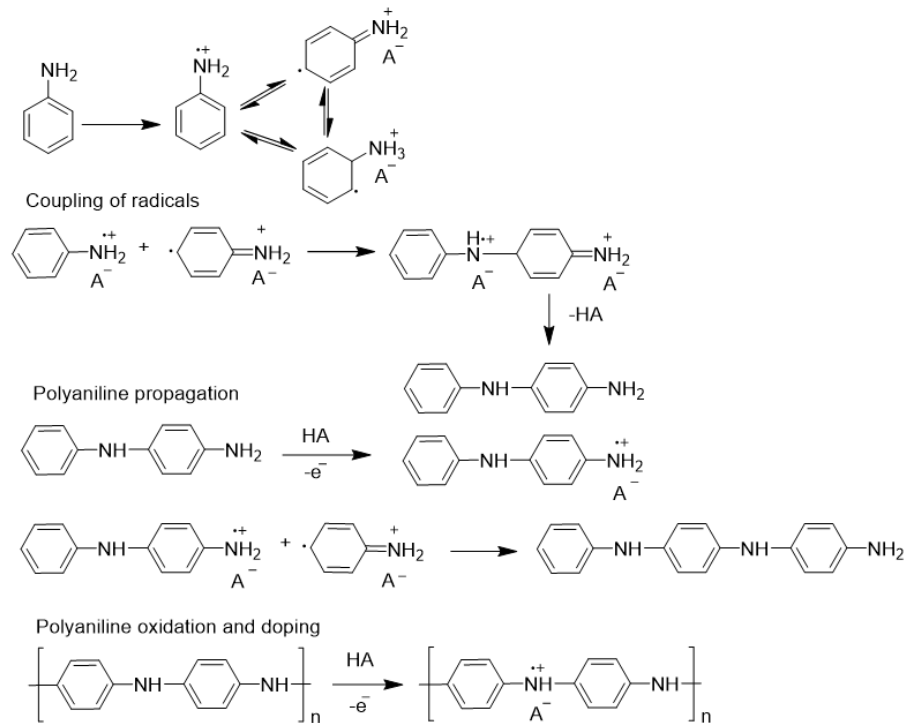


Figure 5. Proposed mechanism of aniline oxidation and PANI formation.⁹

A number of different products can be produced depending on the reaction parameters such as pH, concentration, temperature, oxidant state, and the ratio of monomer-to-oxidant.¹⁰

I.4. Charge transport properties in conducting polymers

Understanding of the charge-carrier transport phenomena in polymers can be derived from understanding the transport properties in single crystals with well-defined packing structures. Conjugated polymer (i.e. PANI) films are typically disordered with some small ordered domains embedded. The interchain interaction is difficult to control and often serves as roadblocks for charge transport.¹¹

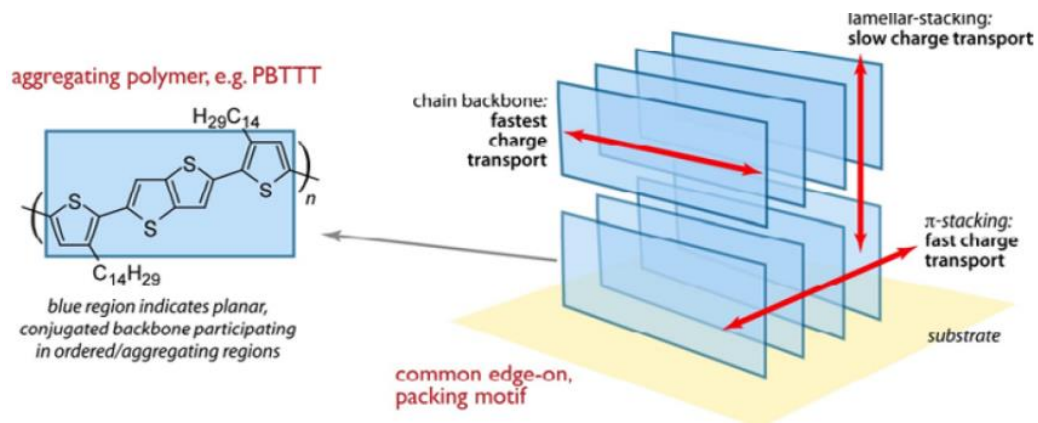


Figure 6. Typical π - π edge-on packing observed for classical semicrystalline polymers.¹¹

Classical semicrystalline polymers have three major charge transport routes as depicted in Figure 6: transport along lamellar-stacking, π - π stacking, and backbone. Lamellar- and π - π stacking results in short-range aggregates or long-range crystallites depending on the chemical nature of polymers and processing conditions.¹¹ The bulk conductivity σ in conjugated polymer is a function of:

$$\sigma = f(\sigma_{\text{intrachain}}); f(\sigma_{\text{interchain}}); f(\sigma_{\text{domain}})$$

where:

- $f(\sigma_{\text{intrachain}})$ is intrachain conductivity along conjugated backbone
- $f(\sigma_{\text{interchain}})$ is interchain conductivity between adjacent polymer chains
- $f(\sigma_{\text{domain}})$ is domain conductivity between domains (can be crystalline or amorphous) of conjugated polymers

Oligomers typically have high interchain conductivity because of their high crystallinity, which allows significant overlap between π -orbitals of adjacent molecules. As a result, an efficient charge carrier transport is formed along the π - π stacking direction. This concept has been demonstrated on nanostructures of aniline tetramers (Figure 7). An up to 2 orders of magnitude enhancement in conductivity compared to the highest previously reported value has been reported in well-ordered tetraaniline single crystals.⁷

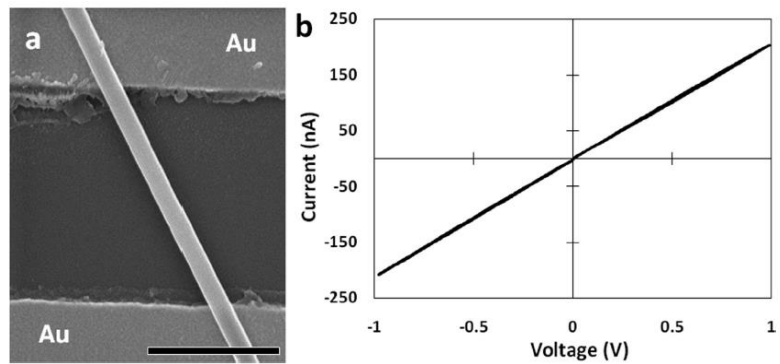


Figure 7. Single TANI nanowire on a Si substrate. 7a) SEM image of an Au bottom-contact device constructed from a single TANI nanowire on a Si substrate
7b) A typical I-V curve for a single nanowire device through a two-probe measurement.
Scale bar = 1 μm .⁷

References

- 1) Ibanez, J. G. Rincón, M. E. Gutierrez-Granados, S. Frontana-Uribe, B. Chem. Rev. 118, **2018**, 4731–4816.
- 2) Kleinschmidt, A. T. Lipomi, D. J. Chem. Rev.117, **2017**, 6467–6499.
b) Kayser, L. V. Lipomi, D. J. Adv. Mater. 31, **2019**, 2-13.
- 3) Wang, B. Yang, W, Mckittrick, J, Prog. Mater. Sci. 76, **2016**, 229-318.
3a) Yu, Y. Yang, W. Meyers, M. A. Mater. Sci. Eng. C. 73, **2017**, 152-163. 3b) Baraldi, A. Jones, S. A. Murdan, S. Pharm Res. 32, **2015**, 1626-1633.
- 4) Fraser, R.D. Parry, David. J. Struct. Biol. **173**, 2011, 391–405.
- 5) Letheby, H. J. Chem. Soc. 15, **1862**, 161-163.
- 6) Wei, Z. Faul, C. Macromol. Rapid Commun. 29, **2008**, 280-292.
- 7) Wang, Y. Tran, H. Kaner, R. J. Am. Chem. Soc. 132, **2010**, 10365–10373.
- 8) Thanh-Hai, T. Kim, Y. Yoon, H. Polymers. 9, **2017**,1-32.
- 9) Naveen, M. Gurudatt, N. G. Yoon-Bo, S. Appl. Mater. Today. 9, **2017**, 419–433.
- 10) Tran, H. D. D'Arcy, J. M. Wang, Y. Richard B. K. J. Mater. Chem. 21, **2011**, 3534–3550.
- 11) Noriega, R. Rivnay, J. Vandewal, K. Nat. Mater. 12, **2013**, 1038-1044.

CHAPTER II. Synthesis of TANI oligomers

II.1. The abbreviation of all TANI oligomers used in this study

Table 1 contains a summary of the molecular structures and the abbreviations of all compounds used in this thesis. The synthesized compounds are shown

Table 1. Summary of molecular structures and abbreviations of compounds in this thesis

Abbr.	LE Compounds	EB Compounds	Abbr.
1LE ¹			1EB ¹
2LE ¹			2EB ¹
3LE ¹			3EB ¹
4LE ¹			4EB
5LE ¹			5EB
6LE ¹			6EB

¹ Synthesized compounds

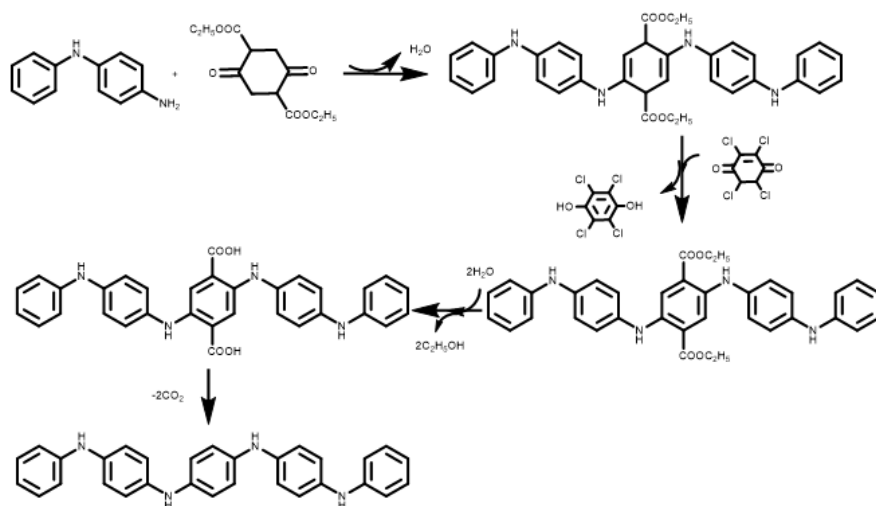
A number of synthetic routes for tetraaniline oligomers (TANI) in leucoemeraldine base form have been developed by other groups.¹⁻⁸ The remainder of this chapter will be focused on the examples of Ph/Ph end-capped tetraaniline oligomers that have been reported so far because of their high conductivity and stability. Subsequently, we will describe the general procedure for making various derivatives of Ph/Ph end-capped TANI with different side-chains or fused ring moieties, followed by their characterization.

A set of Ph/Ph end-capped tetraaniline derivatives with different aromatic central building blocks have been synthesized to study how central aromatic core affects structure-property relationships. In this study, we focused on Ph/Ph end-capped TANIs for two reasons:

- Ph/Ph end-capped oligomers are less reactive than Ph/NH₂ and NH₂/NH₂ end-capped oligomers due to the relatively inert nature of phenyl ring at both ends, leading to excellent environmental stability.
- Tetraaniline oligomers have fewer isomeric forms than the higher oligomers. Their lengths are the same as the smallest repeating unit (four units) for polyaniline, rendering them an effective model system.

II.2. Synthetic routes for making Ph/Ph end-caped TANI in leucoemeraldine oxidation state

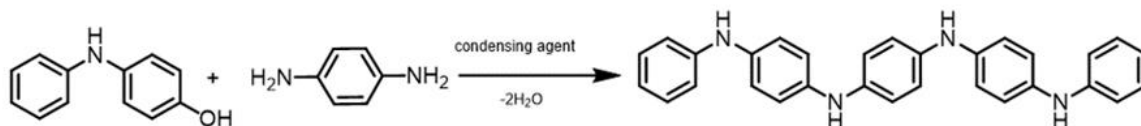
Shortly after polyaniline was discovered to be an electric conductor, Honzl et al.¹ reported the synthesis of the first Ph/Ph end-caped TANI with defined chain length through a condensation reaction between N-phenyl-p-phenylenediamine and diethyl succinoylsuccinate.² Schematic synthesis of Ph/Ph end-caped tetramers has been illustrated below (Scheme 1). This synthetic method contains multiple complicated steps which make the synthesis relatively difficult compared to other methods.



Scheme 1. Summary of Ph/Ph end-caped TANI-LE synthesis of Honzl.²

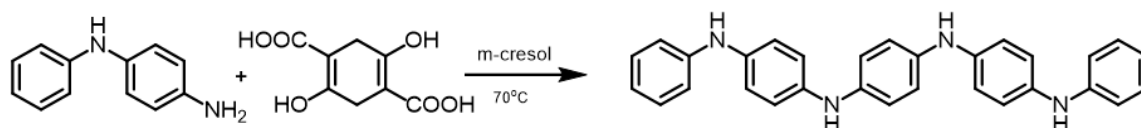
Ochi et al.³ published a second synthetic process for Ph/Ph end-capped TANIs which was a condensation reaction between 4-hydroxydiphenylamine

which is not commercially available and benzene-1,4-diamine, heated in benzene at 70°C for 3 days; titanium alkoxide was used as condensing agent. The final product was extracted with dioxane and collected as silver-white microscopic crystals. Schematic synthesis of Ph/Ph end-capped tetramer based on the Ochi approach has been illustrated below (Scheme 2). While this method was efficient, it suffered from relatively long reaction time.



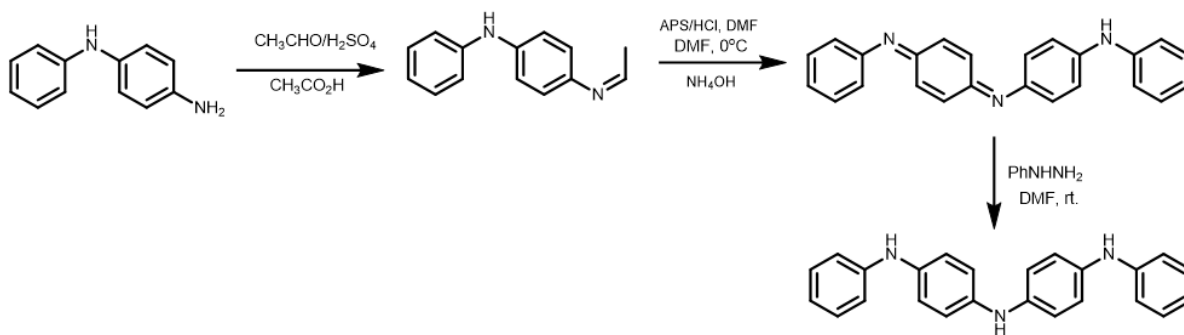
Scheme 2. Summary of Ochi synthesis of Ph/Ph end-caped TANI-LE.³

In a related work, in 1997 Rebourt et al.⁴ introduced a procedure for making Ph/Ph end-capped tetraaniline based on the modification of the Honzl synthetic method. In this method, the condensation reaction was between N-phenyl-p-phenylenediamine and 2,5-dihydroxycyclohexa-1,4-diene-1,4-dicarboxylic acid in meta-cresol at 70°C. He also succeeded in using tetraaniline to make longer oligomers (octaaniline). ¹³C-NMR was in good agreement with the expected structure of Ph/Ph end-caped TANI-LE. The synthetic scheme of Ph/Ph end-capped tetramer based on the Rebourt approach is illustrated in Scheme 3.



Scheme 3. Summary of Rebourt synthesis of Ph/Ph end-caped TANI-LE.⁴

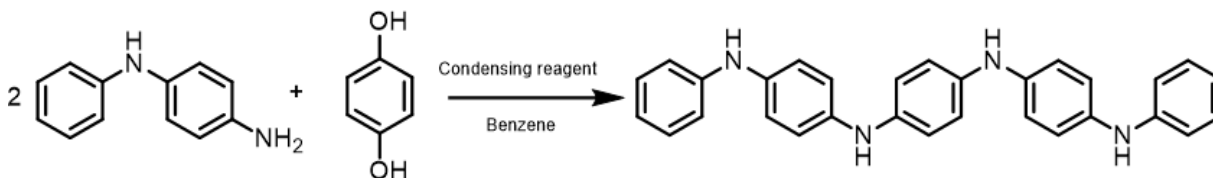
Gao and MacDiarmid in 1999 developed a pseudo-high dilution condition for the synthesis of the phenyl-capped aniline oligomer in the LE oxidation state.⁵ This reaction contains several steps. The first step of this reaction involves the reaction of the acetaldehyde with 1,4-phenylenediamine to form imine derivatives by following oxidative coupling reactions with phenylhydrazine to form the final product. The final product was analyzed by mass spectroscopy (MALDI-TOF-MS) and was in good agreement with the chemical structures of Ph/Ph end-caped TANI-LE. The synthetic scheme is summarized in Scheme 4.



Scheme 4. Summary of Gao synthesis of Ph/Ph end-capped TANI-LE.⁵

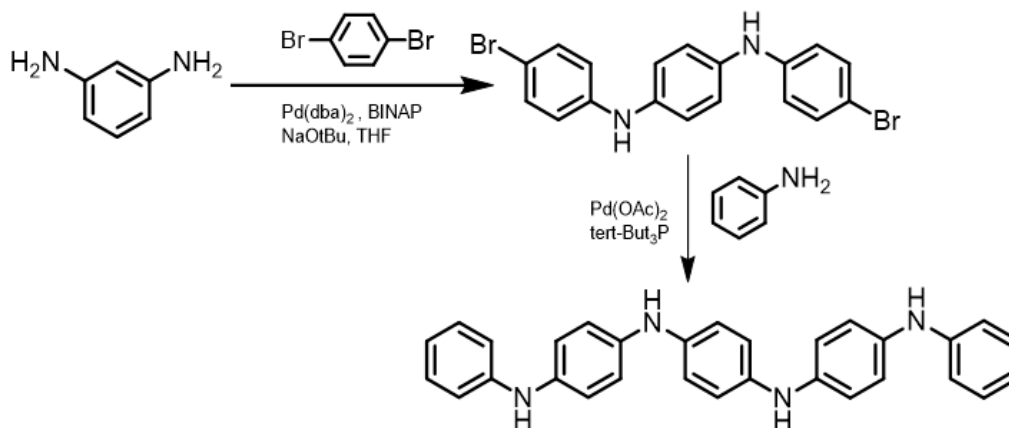
Wei and MacDiarmid in 2002 introduced a new approach for the synthesis of the Ph/Ph TANI oligomer.

Compared to previously reported methods their method was more convenient for making the TANI oligomer.⁶ Liquid titanium (IV) n-butoxide was used as a condensing reagent. The final product was characterized by elemental analysis, UV-vis, and mass spectroscopy and was in good agreement with the expected chemical structure. The synthetic condition is depicted in Scheme 5.



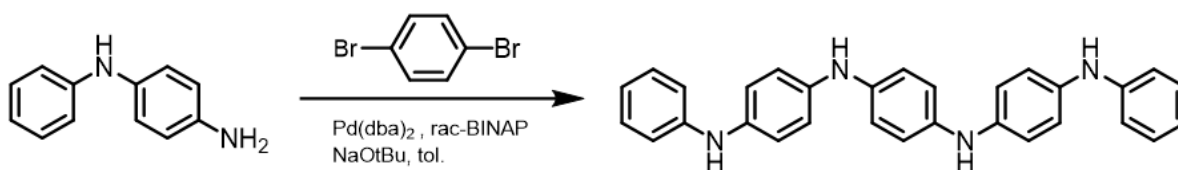
Scheme 5. Summary of MacDiarmid synthesis of Ph/Ph end-capped TANI-LE.⁶

Kaczorowski and Twardowski were two scientists who introduced a new synthesis method in 2005. They prepared the Ph/Ph-TANI in LE oxidation state via palladium-catalyzed amination reactions.⁷ Effectively, they obtained the final products in two steps. The summary of the synthesis is depicted below (Scheme 6).



Scheme 6. Summary of Kaczorowski synthesis of Ph/Ph end-capped TANI-LE.⁷

The most recent approach was introduced by Faul in 2011. He developed a synthetic route based on the Buchwald-Hartwig cross-coupling reaction.⁸ This approach requires fewer purification steps compared to the Kaczorowski approach. The key benefit of the approach is that it is a straightforward way to prepare various derivatives of Ph/Ph end-capped TANI-LE oligomers. The schematic synthesis of Ph/Ph end-capped TANI oligomers based on the Faul approach is summarized in Scheme 7. Because of the simplicity and high yield of this approach, we adopted this route for our synthesis of various TANI derivatives.

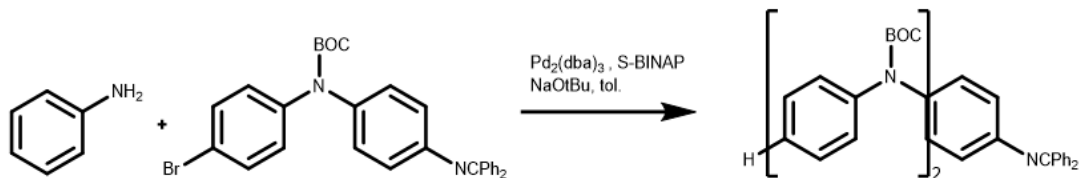


Scheme 7. Summary of Faul synthesis of Ph/Ph end-capped TANI-LE.⁸

II.3. Buchwald-Hartwig cross-coupling reaction

Several synthetic methods have been developed for making carbon-nitrogen bonds.⁹ Among these methods, the simplest one is the Buchwald-Hartwig coupling reaction which is catalyzed by transition metal complexes through the facile amination of aryl halides and aryl-pseudohalides, as shown in Scheme 8. The clear advantages of this method for making C-N bonds, that

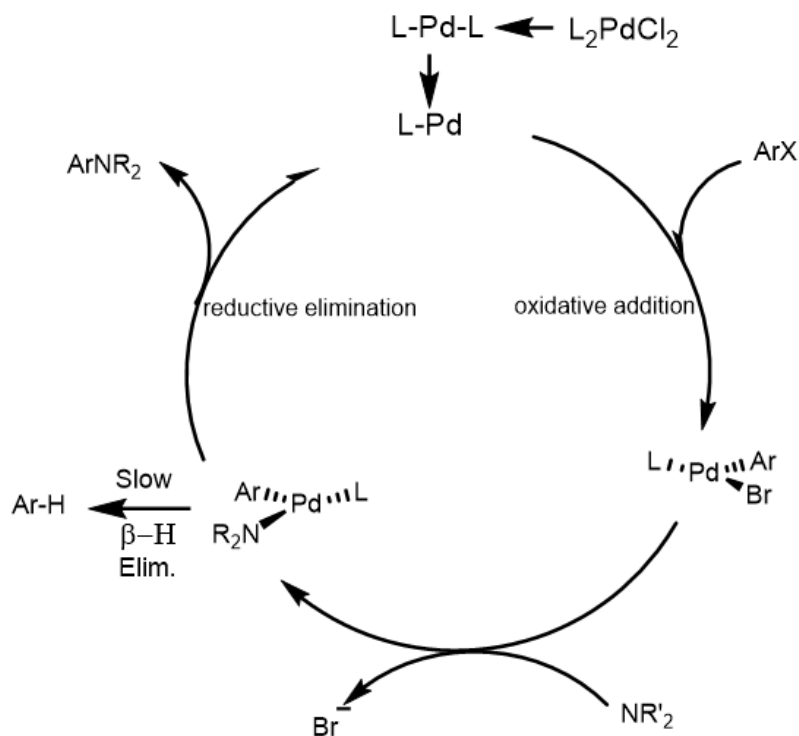
make it remarkable over the other methods are: The high efficiency of the catalyst system, ease of use, stability, and commercial availability of ligands and substrate scope.¹⁰ In particular, this cross-coupling reaction is an effective method for the synthesis of aniline oligomers through C-N formation.¹ Moreover, this reaction has been found to have applications in the pharmaceutical industry and material science.¹⁰



Scheme 8. Palladium-catalyzed coupling reaction for oligoaniline synthesis.¹⁰

II.3.1 Catalytic cycle

The catalytic cycle is described in Scheme 9.¹¹ Initially, aryl halide has been added to the Pd(0) complex in the oxidative addition step. In the next step, the base takes the amine hydrogen and the deprotonated amine coordination to the oxidative addition complex, followed by reductive elimination in the last step. The dominant reaction that competes with the reductive elimination step is β hydride elimination.¹²

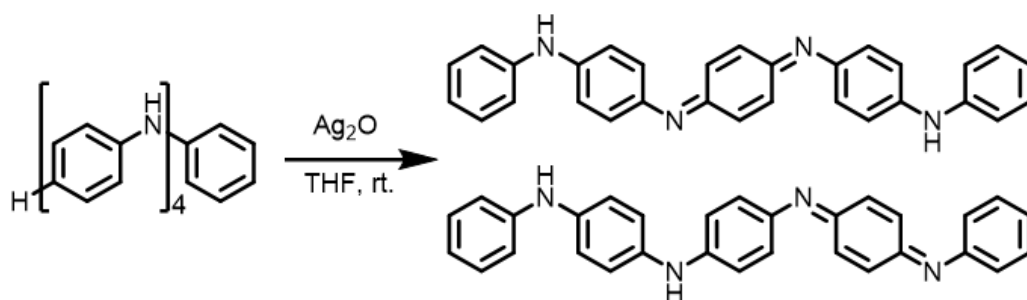


Scheme 9. Catalytic cycle for Buchwald-Hartwig coupling.¹¹

II.4. The oxidation of TANI LE to EB state

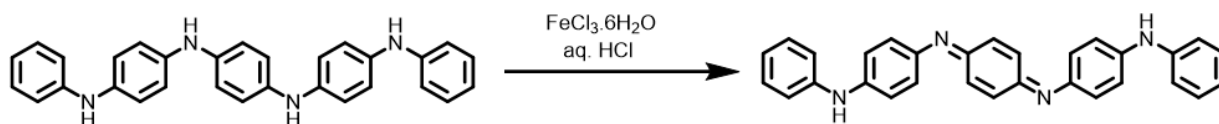
Once the LE form of TANI is synthesized, it needs to be oxidized to the EB form and doped into the ES form to render it electrically conductive. However, this step is delicate, as over-oxidation can easily transition the EB TANI into the pernigraniline oxidation state, which is insulating.

The oxidation reaction of Ph/Ph end-capped TANI-LE with silver(I) oxide in THF to afford Ph/Ph end-capped TANI-LE was reported in 1997. Rebourt et al.⁴ appears to be the first group to announce the synthesis of Ph/Ph end-capped TANI-EB. This compound was characterized by UV-vis and mass spectroscopy. ¹H-NMR and ¹³C-HNMR spectroscopy showed the presence of two structural isomers as shown in Scheme 10.



Scheme 10. Possible positional isomers for Ph/Ph end-capped TANI oligomer.⁴

Wei and MacDiarmid developed a second synthetic process for Ph/Ph end-capped TANI in the EB oxidation state.⁶ This compound was synthesized by the addition of $\text{FeCl}_3 \cdot 6\text{H}_2\text{O}$ in $\text{HCl}_{(\text{aq.})}$ to its LE form (Scheme 11). The final product was characterized by elemental analysis, UV-vis, and mass spectroscopy. No $^1\text{H-NMR}$ spectroscopy was reported for this compound.



Scheme 11. Summary of the Ph/Ph end-capped TANI-EB synthesis.⁶

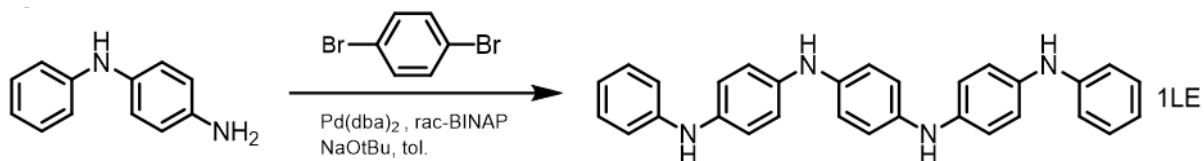
II.5. Synthetic procedures for various Ph/Ph end-capped TANI

Synthesis procedure for making LE compounds (1-6LE) and EB compounds (1-3EB) are described here.

II.5.1. Preparation of the $\text{N}^1, \text{N}^{1'}$ -(1,4-phenylene)-bis(N^4 -phenylbenzene-1,4-diamine) (1LE)

The synthesis of this molecule was performed by a slight modification of literature procedures.⁸ In a flame dried round-bottom flask, N-phenyl-1,4-phenylenediamine (1.64 g, 8.90 mmol, 2.1 eq), 1,4-dibromobenzene (1.00 g, 4.24 mmol, 1 eq), and sodium tert-butoxide (1.22 g, 12.71 mmol, 3 eq) were dissolved in 140 ml toluene and purged with nitrogen flow for 30 min. $[\text{Pd}(\text{dba})_2]$ (0.194 mg, 0.21 mmol, 0.05 eq), rac-BINAP (0.396 mg, 0.636 mmol, 0.15 eq) were added to the solution and it was allowed to reflux at 110°C under nitrogen overnight. TLC taken after 24 hours indicated complete consumption of 1,4-dibromobenzene and showed the major product is likely 1LE. The solution was cooled to room temperature and 5 eq. of phenylhydrazine was added (2.29 g,

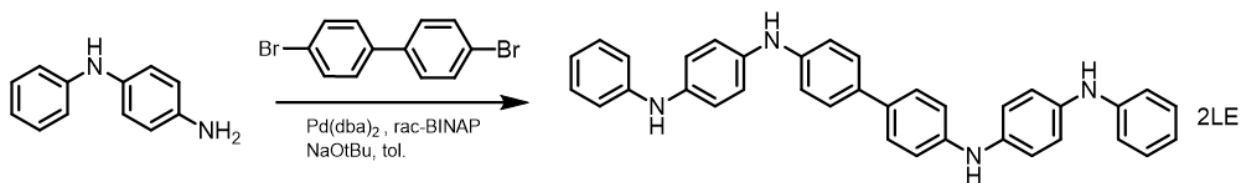
2.08 ml, 21.2 mmol) to the dark purple solution which caused the solution to turn brown. The solution concentrated under reduced pressure. After concentration, the remaining solid was diluted with a mixture of 300 ml ethanol and 60 ml deionized water. After stirring for an hour at room temperature the precipitate was collected by a fine frit and washed with ethanol to remove any residual N-phenyl-1,4-phenylenediamine. The solid collected and dried on the vacuum to afford the green-olive product in the leucoemeraldine base state (1.7 g, 91% yield). This crude product was characterized by $^1\text{H-NMR}$ and UV-vis spectroscopy. Scheme 12 shows a summary of the synthesis of the 1LE.



Scheme 12. Summary of the 1LE synthesis.⁸

II.5.2. Preparation of the N¹, N^{1'}-(biphenyl-4,4'-diyl)-bis(N⁴-phenylbenzene-1,4-diamine) (2LE)

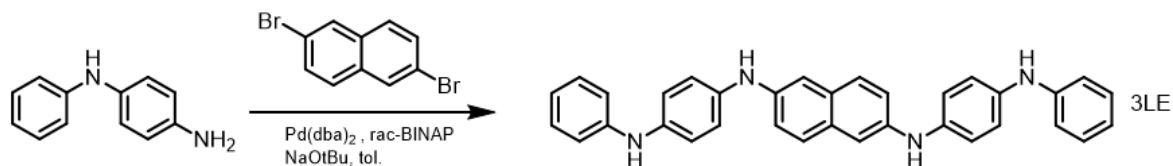
The synthesis of this molecule was performed by a slight modification of literature procedures.⁸ In a flame dried round-bottom flask N-phenyl-1,4-phenylenediamine (1.36 g, 7.37 mmol, 2.3 eq), 4,4'-dibromobiphenyl (1.00 g, 3.2 mmol, 1 eq), and sodium tert-butoxide (0.92 g, 9.6 mmol, 3 eq) were dissolved in 145 ml toluene and purged with nitrogen flow for 30 min. [Pd (dba)₂] (146 mg, 0.16 mmol, 0.05 eq), rac-BINAP (298 mg, 0.48 mmol, 0.15 eq) were added to the solution and it was refluxed at 110°C under nitrogen overnight. TLC after 24 hours indicated complete consumption of 4,4'-dibromobiphenyl and showed the major product is likely 2LE. The solution was cooled to room temperature and phenylhydrazine (1.57 ml, 16 mmol, 5 eq) was added to the solution which caused the solution to turn brown. The solution was concentrated under reduced pressure. After concentration, the remaining solid was diluted with a mixture of 300 ml ethanol and 60 ml deionized water. After stirring for an hour at room temperature the precipitate was collected by fine frit and washed with ethanol to remove any residual N-phenyl-1,4-phenylenediamine. The solid was collected and dried on the vacuum to afford the dark brown product in the leucoemeraldine base state (1.35 g, 84% yield). This crude product was characterized by $^1\text{H-NMR}$ and UV-vis spectroscopy. Scheme 13 shows a summary of the synthesis of the 2LE.



Scheme 13. Summary of the 2LE synthesis.⁸

II.5.3. Preparation of the N¹, N^{1'}-(naphthalene-2,6-diyl)-bis(N⁴-phenylbenzene-1,4-diamine) (3LE)

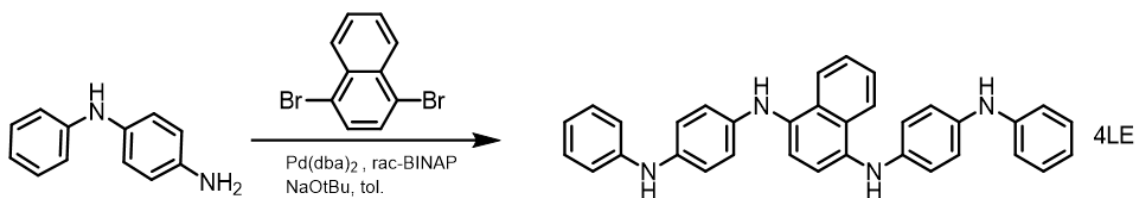
The synthesis of this molecule was performed by a slight modification of literature procedures.⁸ In a flame dried round-bottom flask N-phenyl-1,4-phenylenediamine (2.03 g, 11 mmol, 2.1 eq), 2,6-dibromonaphthalene (1.5 g, 5.24 mmol, 1 eq), and sodium tert-butoxide (1.51 g, 15.72 mmol, 3 eq) were dissolved in 175 ml toluene and purged with nitrogen flow for 30 min. [Pd (dba)₂] (180 mg, 0.31 mmol, 0.06 eq), rac-BINAP (290 mg, 0.47 mmol, 0.09 eq) was added to the solution and the mixture was refluxed at 110°C under nitrogen overnight. TLC after 24 hours indicated complete consumption of 2,6-dibromonaphthalene and showed the major product is likely 3LE. The solution cooled to room temperature and phenylhydrazine (2.59 ml, 26.2 mmol, 5 eq) was added to the solution which caused the solution to turn brown. The solution was concentrated under reduced pressure. After concentration, the remaining solid was diluted with a mixture of 350 ml ethanol and 80 ml deionized water. After stirring for an hour at room temperature the precipitate was collected by fine frit and washed with ethanol to remove any residual N-phenyl-1,4-phenylenediamine. The solid was collected and dried on the vacuum to afford the dark green product in the leucoemeraldine base state (2.12 g, 83%). This crude product was characterized by ¹H-NMR and UV-vis spectroscopy. Scheme 14 shows a summary of the synthesis of the 3LE.



Scheme 14. Summary of the 3LE synthesis.⁸

II.5.4. Preparation of the N¹, N^{1'}-(naphthalene-1,4-diyl)-bis(N⁴-phenylbenzene-1,4-diamine) (4LE)

The synthesis of this molecule was performed by a slight modification of literature procedures.⁸ In a flame dried round-bottom flask N-phenyl-1,4-phenylenediamine (1.35 g, 7.34 mmol, 2.1 eq), 1,4-dibromonaphthalene (1.00 g, 3.49 mmol, 1 eq), and sodium tert-butoxide (1.00 g, 10.47 mmol, 3 eq) were dissolved in 130 ml toluene and purged with nitrogen flow for 30 min. [Pd (dba)₂] (160 mg, 0.17 mmol, 0.06 eq), rac-BINAP (326 mg, 0.52 mmol, 0.09 eq) were added to the solution and the mixture was refluxed at 110°C under nitrogen overnight. TLC taken after 24 hours indicated complete consumption of 1,4-dibromonaphthalene and showed the major product is 4LE. The solution was cooled to room temperature and phenylhydrazine (1.71 ml, 17.45 mmol, 5 eq) was added to the solution which caused the solution to turn brown. The solution was concentrated under reduced pressure. After concentration, the remaining solid was diluted with a mixture of 300 ml iso-propane and 60 ml deionized water. After stirring for an hour at room temperature, the precipitate was collected by fine frit and washed with ethanol to remove any residual N-phenyl-1,4-phenylenediamine. The dark purple solid was collected and dried on the vacuum to afford the purple product in the leucoemeraldine base state (1.25 g, 93% yield). This crude product was characterized by ¹H-NMR and UV-vis spectroscopy. Scheme 15 shows a summary of the synthesis of the 4LE.

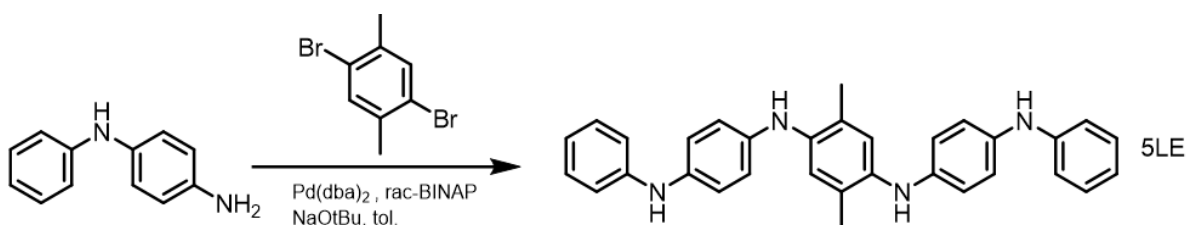


Scheme 15. Summary of the 4LE synthesis.⁸

II.5.5. Preparation of the N¹, N^{1'}-(2,5-dimethyl-1,4-phenylene)-bis(N⁴-phenylbenzene-1,4-diamine) (5LE)

In a flame dried round-bottom flask N-phenyl-1,4-phenylenediamine (1.46 g, 7.95 mmol, 2.1 eq), 1,4-dibromo-2,5-dimethylbenzene (1.00 g, 3.78 mmol, 1 eq), and sodium tert-butoxide (1.09 g, 11.36 mmol, 3 eq) were dissolved in 140 ml toluene and purged with nitrogen flow for 30 min. [Pd (dba)₂] (173 mg, 0.19 mmol, 0.06 eq), rac-BINAP (354 mg, 0.57 mmol, 0.09 eq) were added to the solution and the mixture was refluxed at 110°C under nitrogen overnight. TLC taken after 24 hours indicated complete consumption of 1,4-dibromo-2,5-dimethylbenzene and showed the major product is 5LE. The solution was cooled

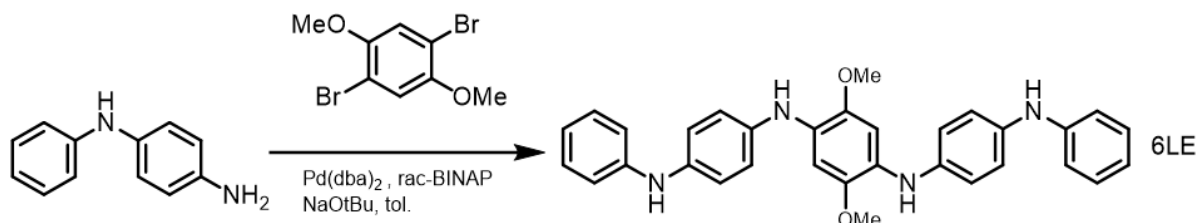
to room temperature and phenylhydrazine (1.84 ml, 18.75 mmol, 5 eq) was added to the solution which caused the solution to turn brown. The solution was concentrated under reduced pressure. After concentration, the remaining solid was diluted with a mixture of 300 ml ethanol and 60 ml deionized water. After stirring for an hour at room temperature the precipitate was collected by fine frit and washed with ethanol to remove any residual N-phenyl-1,4-phenylenediamine. The brown solid was collected and dried on the vacuum to afford the product in the leucoemeraldine base state (1.2 g, 89% yield). This crude product was characterized by ¹H-NMR and UV-vis spectroscopy. Scheme 16 shows a summary of the synthesis of the 5LE.



Scheme 16. Summary of the 5LE synthesis.

II.5.6. Preparation of the N¹, N^{1'}-(2,5-dimethoxy-1,4-phenylene)-bis(N⁴-phenylbenzene-1,4-diamine) (6LE)

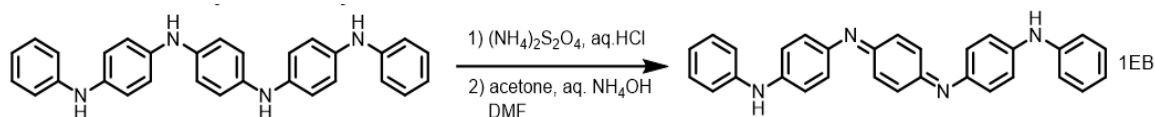
In a flame dried round-bottom flask N-phenyl-1,4-phenylenediamine (1.31 g, 7.09 mmol, 2.1 eq), 1,4-dibromo-2,5-dimethoxybenzene (1.00 g, 3.38 mmol, 1 eq), and sodium tert-butoxide (0.975 g, 10.14 mmol, 3 eq) were dissolved in 140 ml toluene and purged with nitrogen flow for 30 min. [Pd (dba)₂] (155 mg, 0.17 mmol, 0.06 eq), rac-BINAP (315 mg, 0.51 mmol, 0.09 eq) added to the solution and the mixture was refluxed at 110°C under nitrogen overnight. TLC after 24 hours indicated complete consumption of 1,4-dibromo-2,5-dimethoxybenzene and showed the major product is 6LE. The solution was cooled to room temperature and phenylhydrazine (1.66 ml, 16.9 mmol, 5 eq) was added to the solution which caused the solution to turn brown. The solution was concentrated under reduced pressure. After concentration, the remaining solid was diluted with a mixture of 300 ml ethanol and 60 ml deionized water. After stirring for an hour at room temperature the precipitate was collected by fine frit and washed with ethanol to remove any residual N-phenyl-1,4-phenylenediamine. The brown solid was collected and dried on the vacuum to afford the product in the leucoemeraldine base state (1.17 g, 85% yield). This crude product was characterized by ¹H-NMR and UV-vis spectroscopy. Scheme 17 shows a summary of the synthesis of the 6LE.



Scheme 17. Summary of the 6LE synthesis.

II.5.7. Preparation of the 4,4'-(((1E,4E)-cyclohexa-2,5-diene-1,4-diylidene)-bis(azaneylylide)-bis(N-phenylaniline)) (1EB)

The synthesis of this molecule was performed by a slight modification of literature procedures.⁸ 1LE compound was oxidized to 1EB based on the previously reported method. In the round bottom flask, 1LE (0.219 g, 0.49 mmol, 1 eq) was dissolved in 50 ml DMF and stirred for 10 min at room temperature. A solution of ammonium persulfate (0.118 g, 0.49 mmol, 1 eq) in hydrochloric acid (16 mL, 2 M) was added in a single portion to the round bottom flask solution and stirred for one minute. Deionized water (250 ml) was added to the solution and stirred for 15 min, resulting in a deep green precipitate. The resulting solution was filtered through a fine frit and treated with 80 ml acetone and ammonium hydroxide (40 ml, 2M). After stirring for 20 min at room temperature the deep purple solid was collected by fine frit and dried under vacuum to afford the final product in the emeraldine base form (143 mg, 67% yield). This crude product was characterized by ¹H-NMR and UV-vis spectroscopy. Scheme 18 shows a summary of the synthesis of the 1EB.

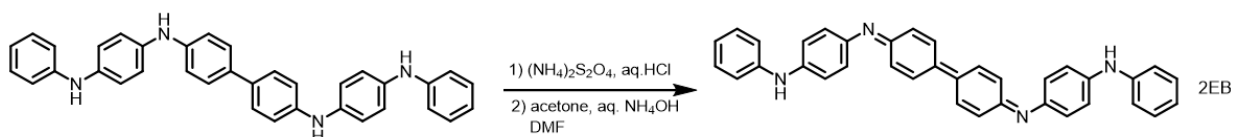


Scheme 18. Summary of the 1EB synthesis.⁸

II.5.8. Preparation of the 4,4'-(((1E,4E,4'E)-[1,1'-bi(cyclohexylidene)]-2,2',5,5'-tetraenylidene-4,4'-diylidene)-bis(azaneylylidene))-bis-(N-phenylaniline) (2EB)

The synthesis of this molecule was performed by a slight modification of literature procedures.⁸ 2LE compound was oxidized to 2EB based on the previously reported method. In the round bottom flask, 2LE (0.1 g, 0.19 mmol, 1 eq.) was dissolved in 60 ml DMF and stirred for 10 min at room temperature. A solution of ammonium persulfate (0.044 g, 0.19 mmol, 1 eq) in hydrochloric acid

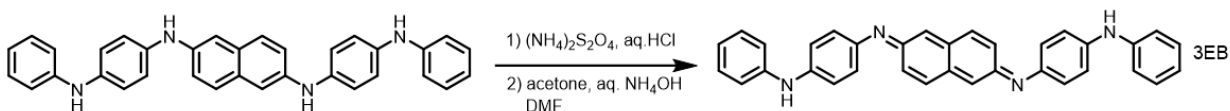
(8 mL, 2 M) was added in a single portion to the round bottom flask solution and stirred for one minute. Deionized water (120 ml) was added to the solution and stirred for 15 min, resulting in a deep green precipitate. The resulting solution was filtered through a fine frit and treated with 40 ml acetone and ammonium hydroxide (20 ml, 2M). After stirring for 20 min at room temperature the deep red-brown solid was collected by fine frit and dried under vacuum to afford the final product in the emeraldine base form (65 mg, 65% yield). This crude product was dissolved in 100 ml ether and filtered through the fine frit. The filtrate was characterized by $^1\text{H-NMR}$ and UV-vis spectroscopy. Scheme 19 shows a summary of the synthesis of the 2EB.



Scheme 19. Summary of the 2EB synthesis.⁸

II.5.9. Preparation of the 4,4'-(((2E,6E)-naphthalene-2,6-diylidene)-bis(azaneylylidene))-bis(N-phenylaniline) (3EB)

The synthesis of this molecule was performed by a slight modification of literature procedures.⁸ 3LE compound was oxidized to 3EB based on the previously reported method. In the round bottom flask, 3LE (0.1 g, 0.20 mmol, 1 eq) was dissolved in 60 ml DMF and stirred for 10 min at room temperature. A solution of ammonium persulfate (0.05 g, 0.22 mmol, 1 eq) in hydrochloric acid (8 mL, 2 M) was added in a single portion to the round bottom flask solution and stirred for one minute. Deionized water (120 ml) was added to the solution and stirred for 15 min that resulted in the deep green precipitate. The resulting solution was filtered through a fine frit and treated with 40 ml acetone and ammonium hydroxide (11 ml, 2M). After stirring for 20 min at room temperature the deep purple solid was collected by fine frit and dried under on the vacuum. This crude product was dissolved in 100 ml diethyl ether and filtered through the fine frit. The filtrate was dried under on the vacuum to afford the final product in the emeraldine base form (67 mg, 67% yield). The final product was characterized by $^1\text{H-NMR}$ and UV-vis spectroscopy. Scheme 20 shows a summary of the synthesis of the 3EB.



Scheme 20. Summary of the 3EB synthesis.⁸

References

- 1) Sadighi, J. Buchwald, S. J. Am. Chem. Soc. 120, **1998**, 4960-4976.
- 2) Honzl, J. M. Tlustakova, J. Polym. Sci.: Part C 22, **1968**, 451.
- 3) Ochi, M. H. Furusho, J. Tanaka, Bull. Chem. Sci. Jpn. 67, **1994**, 1749-1752
- 4) Rebourt, E. Joule, J.A. Monkman, A.P. Synth. Met. 84, **1997**, 65-66.
- 5) Gao, J. Li, k. W. Zhang, W. MacDiarmid, A. G. Polym. Prepr. 40, **1999**, 107.
- 6) Wang, W. MacDiarmid, A. G. Synth. Met. 129, **2002**, 199-205.
- 7) Kaczorowski, R. Twardowski, A. Synthetic Metals. 151, **2005**, 106–113.
- 8) Faul, C. F. J. Chem. Eur. J. 17, **2011**, 12512 – 12521.
- 9) Razzuk, A. Biehl, J. Org. Chem. 52, **1987**, 2619-2622.
- 10) Surry, D.S. Buchwald, S.L. Chem. Sci. 2, **2011**, 27-50.
- 11) Hartwig, J. Frederic, P. J. Am. Chem. Soc. 118, **1996**, 3626-3633.
- 12) Guram, S. Buchwald, S.L. Angew. Chem. Int. Ed. Engl. 34, **1995**, No. 12.

CHAPTER III. Characterization of TANI oligomers

III.1. $^1\text{H-NMR}$ spectroscopy

All NMR experiments were performed on a Bruker 600 MHz NMR at room temperature. All samples were dissolved in dimethyl sulfoxide- d_6 and filtered through a syringe filter before the run to remove undissolved particulates.

III.1.1. Characterization of $\text{N}^1, \text{N}^{1'}\text{-(1,4-phenylene)-bis(N}^4\text{-phenylbenzene-1,4-diamine)}$ (1LE)

$^1\text{H-NMR}$ spectroscopy was performed so that the chemical structure and purity of the compound can be confirmed. A representative $^1\text{H-NMR}$ spectrum of this compound has been included (Figure 8). The hydrogen atom labeling scheme for this compound is shown in the spectrum.

The $^1\text{H-NMR}$ spectrum of this compound displays a singlet at 7.73 ppm that belongs to NH (labeled a), and a singlet at 7.58 ppm that belongs to another NH (labeled b). The positions of the -NH- signals are determined by the character of the neighboring aromatic rings. The peaks related to other protons are also labeled in the molecular structure.

These assignments are consistent with the $^1\text{H-NMR}$ spectrum that was previously reported by Prof. Charl Faul's group.¹

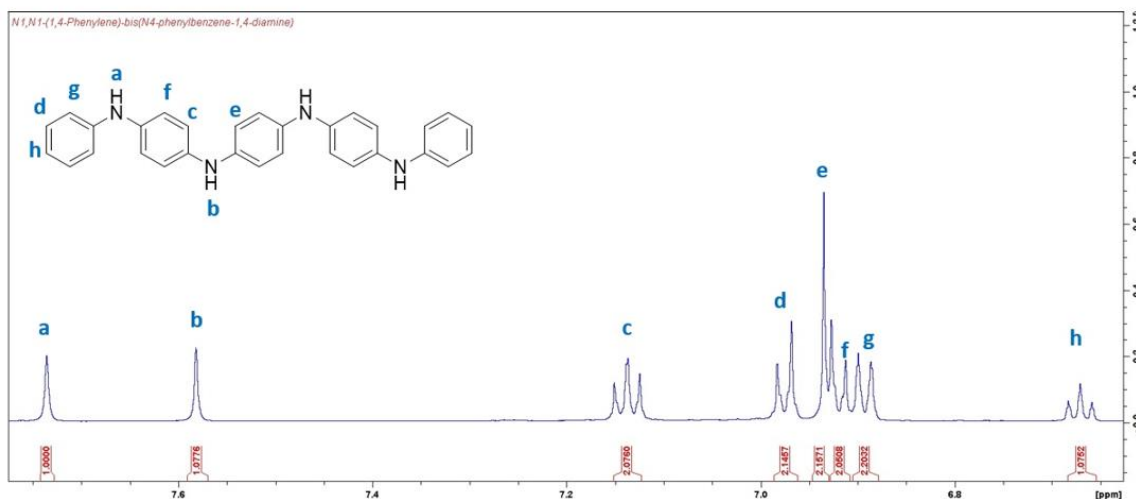


Figure 8. $^1\text{H-NMR}$ spectrum of 1LE compound.

III.1.2. Characterization of the N¹, N^{1'}-(biphenyl-4,4'-diyl)-bis(N⁴-phenylbenzene-1,4-diamine) (2LE)

A representative ¹H-NMR spectrum of this compound has been included (Figure 9). The hydrogen atom labeling scheme for this compound is shown in the spectrum. The ¹H-NMR spectrum of this compound displays a singlet at 7.95 ppm that is attributed to NH (labeled a), and a singlet at 7.87 ppm that belongs to another NH (labeled b). The peaks related to other protons are also labeled in the molecular structure. The observed ¹H-NMR spectrum agrees with the data published previously by Prof. Charl Faul's group.¹

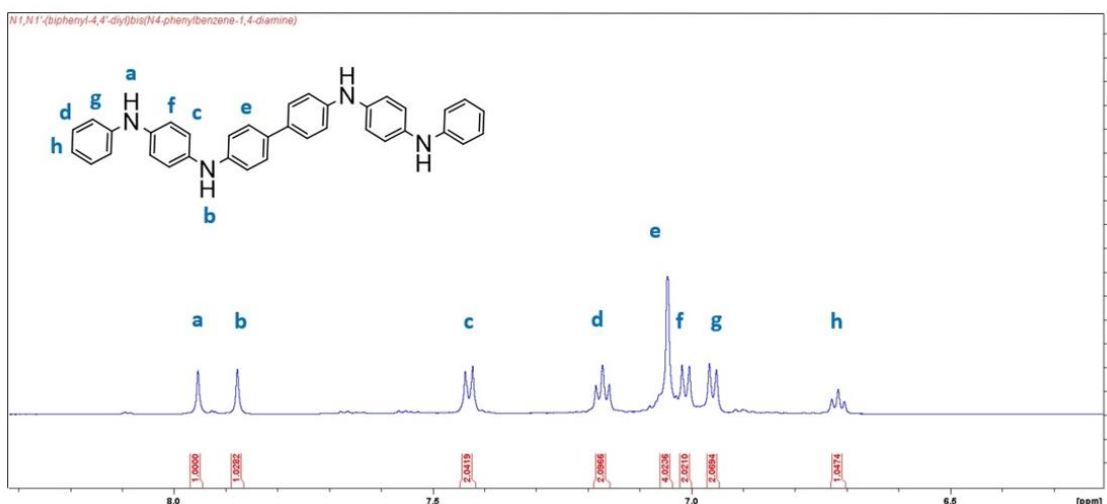


Figure 9. ¹H-NMR spectrum of 2LE compound.

III.1.3. Characterization of the N¹, N^{1'}-(naphthalene-2,6-diyl)-bis(N⁴-phenylbenzene-1,4-diamine) (3LE)

A representative ¹H-NMR spectrum of this compound has been included in Figure 10. The hydrogen atom labeling scheme for this compound is shown in the spectrum. The ¹H-NMR spectrum of this compound displays a singlet at 7.93 ppm that belongs to NH (labeled a), and a singlet at 7.88 ppm that belongs to another NH (labeled b). The peaks related to other protons are also labeled in the molecular structure. The observed ¹H-NMR spectrum agrees with the data published previously by Prof. Charl Faul's group.¹

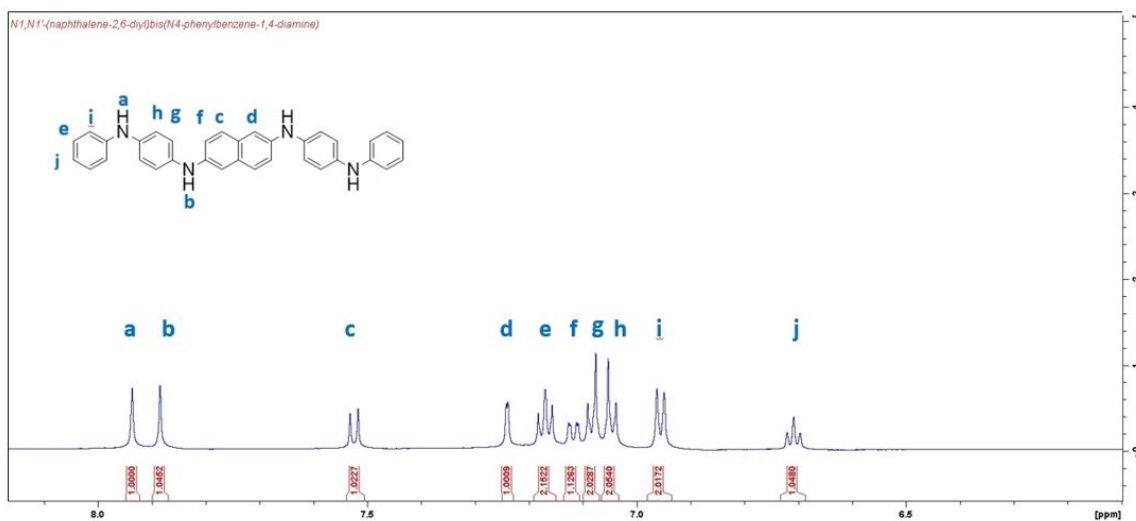


Figure 10. $^1\text{H-NMR}$ spectrum of 3LE compound.

III.1.4. Characterization of $\text{N}^1, \text{N}^{1'}$ -(naphthalene-1,4-diyl)-bis(N^4 -phenylbenzene-1,4-diamine) (4LE)

A representative $^1\text{H-NMR}$ spectrum of this compound has been included in Figure 11. The hydrogen atom labeling scheme for this compound is shown in the spectrum. The $^1\text{H-NMR}$ spectrum of this compound displays a singlet at 8.33 ppm that belongs to amine nitrogen (labeled b). The peaks related to other protons are also labeled in the molecular structure.

The structural information that we obtained from the spectrum revealed that the synthesized 4LE compound is in the emeraldine oxidation state rather than the reduced form. $^1\text{H-NMR}$ of this compound suggests that the 4LE compound may be easily oxidized in polar organic solvents to 4EB. To provide insight into the result obtained, we conducted a UV-vis spectroscopy experiment to clarify the nature of the 4LE compound.

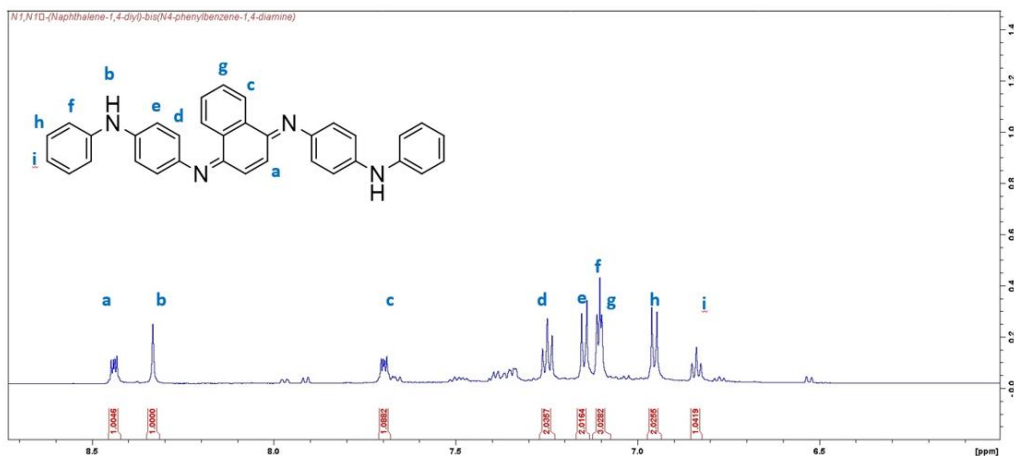


Figure 11. $^1\text{H-NMR}$ spectrum of 4LE compound.

III.1.5. Characterization of $\text{N}^1, \text{N}^{1'}$ -(2,5-dimethyl-1,4-phenylene)-bis(N^4 -phenylbenzene-1,4-diamine) (5LE)

A representative $^1\text{H-NMR}$ spectrum of this compound has been included (Figure 12). The hydrogen atom labeling scheme for this compound is shown in the spectrum. The $^1\text{H-NMR}$ spectrum of this compound displays a singlet at 8.30 ppm that belongs to NH (labeled a), and a singlet at 7.68 ppm that belongs to another NH (labeled b). The peak for methyl hydrogens appeared at 2.20 ppm. A solvent peak (2.50 ppm) and a water peak (3.33 ppm) are obvious in the spectrum. The peaks related to other protons are also labeled in the molecular structure.

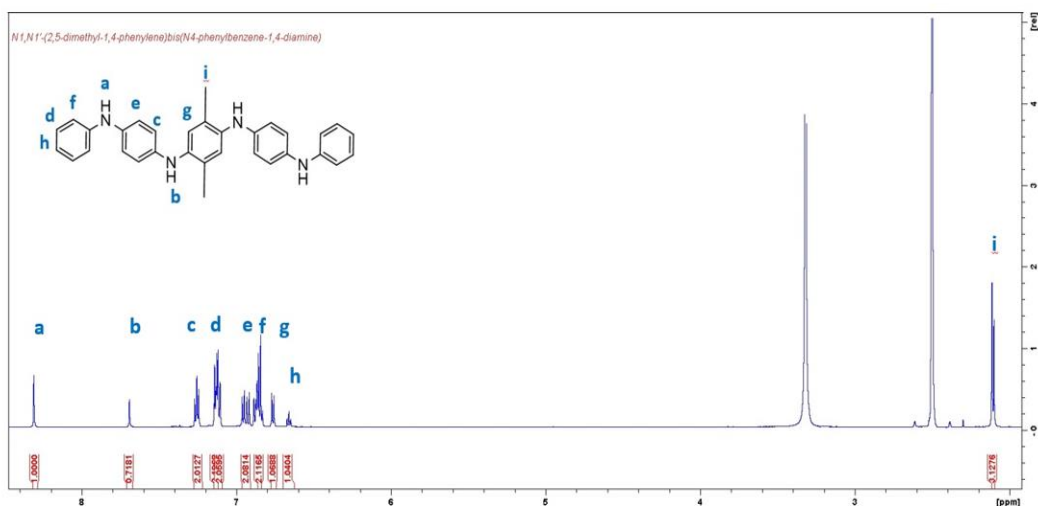


Figure 12. $^1\text{H-NMR}$ spectrum of 5LE compound.

III.1.6. Characterization of the N¹, N^{1'}-(2,5-dimethoxy-1,4-phenylene)-bis(N⁴-phenylbenzene-1,4-diamine) (6LE)

A representative ¹H-NMR spectrum of this compound has been included (Figure 13). The hydrogen atom labeling scheme for this compound is shown in the spectrum. The ¹H-NMR spectrum of this compound displays a singlet at 8.27 ppm that belongs to NH (labeled a). The peak for methoxy hydrogens appeared at 3.6 ppm. The peaks related to other protons are also labeled in the molecular structure.

The structural information that we obtained from the spectrum revealed that the synthesized 6LE compound is in the emeraldine oxidation state rather than the reduced form. ¹H-NMR of this compound suggests that the 6LE compound may be easily oxidized in polar organic solvents to 6EB. To provide insight into the result obtained, we conducted a UV-vis spectroscopy experiment to clarify the nature of the 6LE compound.

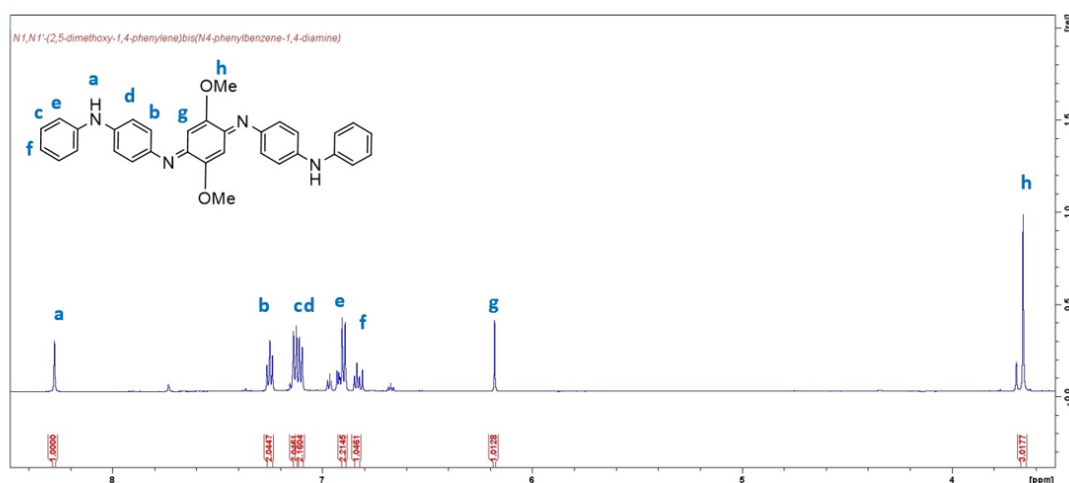


Figure 13. ¹H-NMR spectrum of 6LE compound.

III.1.7. Characterization of the 4,4'-(((1E,4E)-cyclohexa-2,5-diene-1,4-diylidene)-bis(azanelylylde)-bis(N-phenylaniline)) (1EB)

A representative ¹H-NMR spectrum of 1EB compound has been included (Figure 14). The hydrogen atom labeling scheme for this compound is shown in the spectrum. In contrast to the amine signals seen on the fully reduced form of TANI, the existence of a new quinoid ring upon oxidation in the molecular structure results in the loss of one of the amine proton signals relative to the signals observed in the spectrum of the 1LE.

The signals in the 7.9-8.4 ppm region are related to the -N-H groups. The $^1\text{H-NMR}$ spectrum of this compound displays a singlet at 8.38 ppm that belongs to NH (labeled a). It should be noted that the oxidation of the 1EB compound results in a mixture of isomers that was investigated by other groups previously.^{4,13} These two isomeric forms are depicted in Figure 14. The two tiny doublet peaks at 8.26 ppm and 7.93 ppm attributed to NH (labeled b and c) respectively. The relative molar ratio of these two potentially formed isomers is 65:35. The isomer with a quinoidal unit in the center takes the largest ratio. These assignments are consistent with the $^1\text{H-NMR}$ that was previously reported.

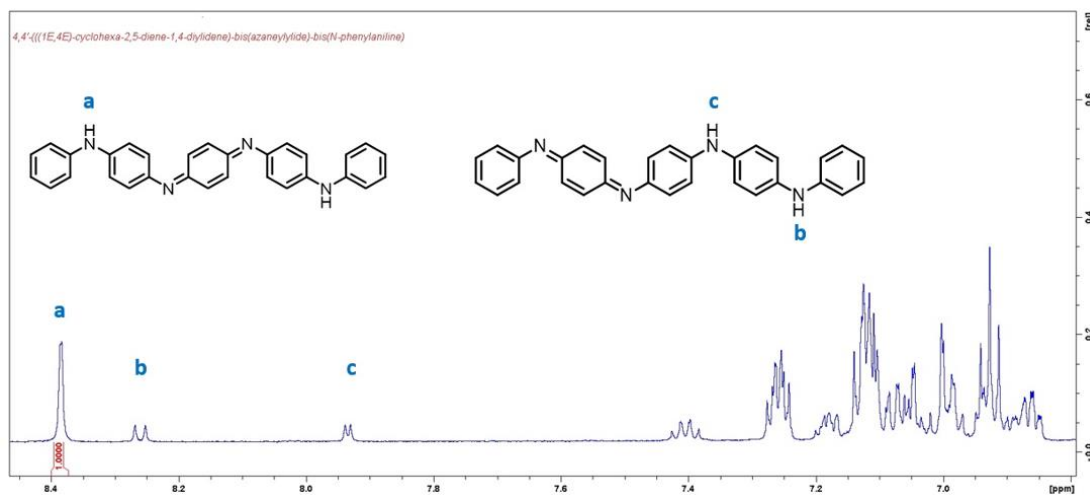


Figure 14. $^1\text{H-NMR}$ spectrum of 1EB compound.

III.1.8. Characterization of the 4,4'-(((1E,4E,4'E)-[1,1'-bi(cyclohexylidene)]-2,2',5,5'-tetraenylidene-4,4'-diylidene)-bis(azaneylylidene))-bis(N-phenylaniline) (2EB)

A representative $^1\text{H-NMR}$ spectrum of 2EB compound has been included (Figure 15). The hydrogen atom labeling scheme for this compound is shown in the spectrum. The $^1\text{H-NMR}$ spectrum of this compound displays a doublet at 8.08 ppm that belongs to NH (labeled a) and another doublet at 7.92 ppm (labeled b). The nature of this second peak was not investigated in this study. Two single peaks (labeled c_1 and c_2) belong to the reduced form (2LE). The ratio of 2EB to 2LE is 71:29.

The $^1\text{H-NMR}$ result suggests that the quantitative oxidation of the 2LE is synthetically challenging and results in a mixture of compounds.

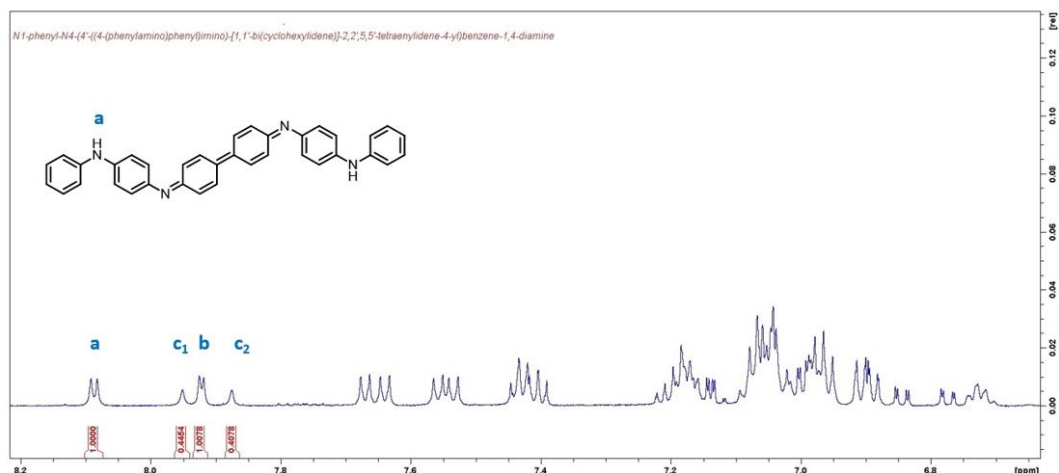


Figure 15. $^1\text{H-NMR}$ spectrum of 2EB compound.

III.1.9. Characterization of the 4,4'-(((2E,6E)-naphthalene-2,6-diyldiene)-bis(azaneylylidene))-bis(N-phenylaniline) (3EB)

A representative $^1\text{H-NMR}$ spectrum of this compound has been included (Figure 16). The hydrogen atom labeling scheme for this compound is shown in the spectrum. The $^1\text{H-NMR}$ spectrum of this compound displays a doublet at 8.24 ppm that belongs to NH (labeled a) and another doublet at 7.96 ppm (labeled b). The nature of this second peak was not investigated in this study. Two single peaks (labeled c_1 and c_2) belong to $-\text{NH}-$ group in 3LE. The ratio of 3EB to 3LE is 56:43.

$^1\text{H-NMR}$ result suggests that the quantitative oxidation of the 3LE is synthetically challenging and results in a mixture of compounds.

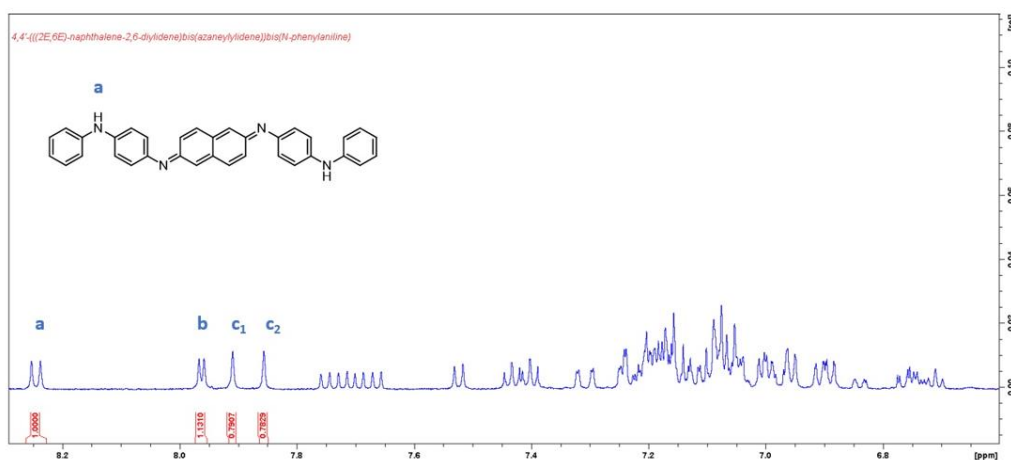


Figure 16. $^1\text{H-NMR}$ spectrum of 3EB compound.

III.2. UV-vis spectroscopy

Six different derivatives of Ph/Ph end capped TANI oligomers in this study have been used to investigate and compare the effects of central aromatic core on optoelectronic properties of TANI oligomers. The UV-vis absorption spectra of TANI compounds in chloroform were taken with a quartz cuvette with a light path length of 1 mm on a Shimadzu UV-3600 Plus spectrophotometer at room temperature. About 1 mg of the samples were dissolved in ~ 1 ml CHCl_3 . UV-vis spectra of leucoemeraldine compounds (1-3LE) are shown in Figure 17. The maximum absorption wavelength peaks are summarized in Table 2.

The UV-vis spectra of these LE compounds show the characteristic absorption maxima at 336 nm, 317 nm, and 330 nm for 2LE, 1LE, and 3LE, respectively. As observed in Figure 17, the reduced state form compounds only show one absorption peak associated with the $\pi \rightarrow \pi^*$ transition in the benzenoid rings.¹

The 2LE shows a sharp peak at the 336 nm maximum absorption peak. The generation of a broad peak ranging from 467-493 nm (indicated by the arrow in Figure 17) for the 2LE compound suggests that this compound is susceptible to be oxidized into the upper oxidation state (2EB) under the current reaction condition. It exhibits a feature typical of the oxidized form that is related to the emeraldine oxidation state. This could be understood by looking at the overlaid spectra of 1-3 LE compounds vs. 1-3EB compounds (Figure 18).

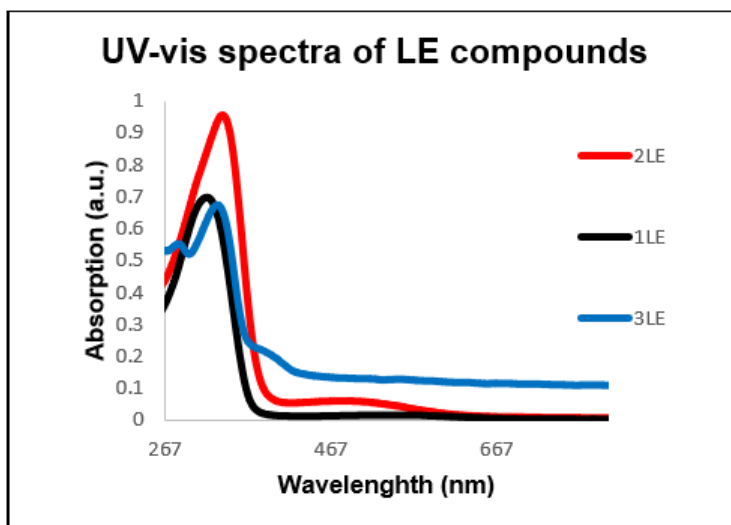
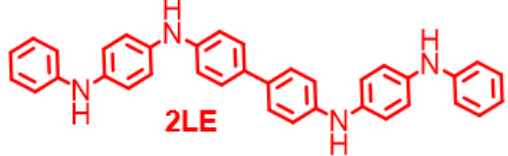
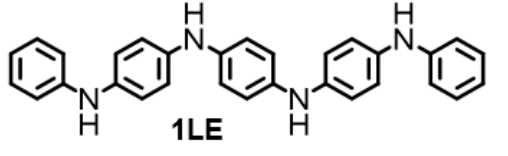
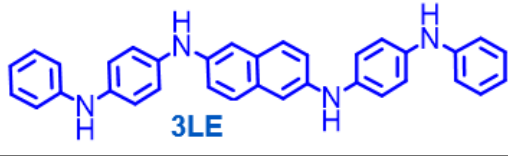


Figure 17. UV-vis absorption spectra of TANI oligomers (1-3) in LE oxidation state in CHCl_3

Table 2. The maximum absorption wavelength peaks for LE compounds (1-3)

Molecular structure of LE compounds	Maximum Absorption
 <p style="text-align: center;">2LE</p>	336 nm
 <p style="text-align: center;">1LE</p>	317 nm
 <p style="text-align: center;">3LE</p>	330 nm 393 nm

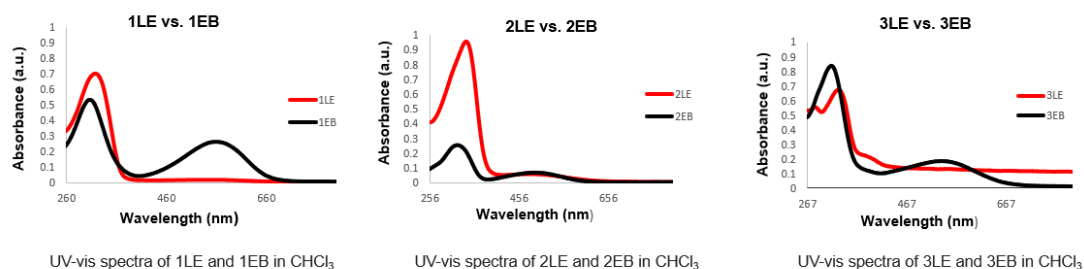


Figure 18. Generation of second absorption peak upon oxidation.

UV-vis spectra of emeraldine base compounds are shown in Figure 19. The maximum absorption wavelength peaks are summarized in Table 3. As observed in Figure 19, the oxidation process leads to new peaks in the longer wavelength region of the spectrum. The emeraldine state of these compounds (1-6EB) shows two absorption peaks. The first peaks at the shorter wavelength (302-317 nm) are associated with the $\pi \rightarrow \pi^*$ transition in the benzenoid rings. Based on the previous theoretical and experimental studies on PANI, the second peak (λ_{2max}) for the 1EB compound has been attributed to $n \rightarrow \pi^*$ transitions, where n refers to nonbonding electrons. Interestingly, a recent study on aniline

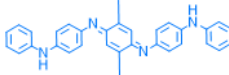
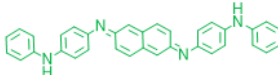
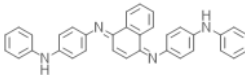
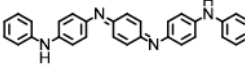
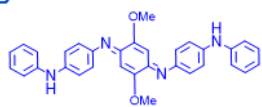
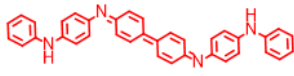
oligomers indicates that ($\lambda_{2\max}$) is a further $\pi \rightarrow \pi^*$ transition. This statement is confirmed by time-dependent density functional theory (TD-DFT) calculations in Faul's group.¹

Shifting toward a larger wavelength (up to 10 nm) in 2EB (317 nm $\lambda_{1\max}$) compared to 1EB (307 nm $\lambda_{1\max}$) is the result of the extended π -conjugation system. With the larger conjugated system, the energy difference between HOMO-LUMO becomes smaller, resulting in lower energy absorption or higher wavelength.

UV-Vis analysis of the 5LE compound in chloroform produces confusing results. In chloroform, it appears that the 5LE also contains some of the 5EB, but NMR opposes this conclusion.

In addition, UV-vis spectra of compounds 4EB, 5EB, and 6EB confirmed that they are in the emeraldine oxidation state with characteristic absorption maxima at 523, 538, and 526 nm, respectively. The presence of the second peak ($\lambda_{2\max}$) unambiguously indicates that all these compounds are in their emeraldine base form.

Table 3. The maximum absorption wavelength peaks for EB compounds (1-6).

Molecular structure of EB compounds	Max absorption
5EB 	$\lambda_{1\max}$ 310 nm $\lambda_{2\max}$ 537.5 nm
3EB 	$\lambda_{1\max}$ 316 nm $\lambda_{2\max}$ 537 nm
4EB 	$\lambda_{1\max}$ 302 nm $\lambda_{2\max}$ 521-526 nm
1EB 	$\lambda_{1\max}$ 306.5 nm $\lambda_{2\max}$ 555-564 nm
6EB 	$\lambda_{1\max}$ 311 nm $\lambda_{2\max}$ 525.5 nm
2EB 	$\lambda_{1\max}$ 316.5 nm $\lambda_{2\max}$ 448-498 nm

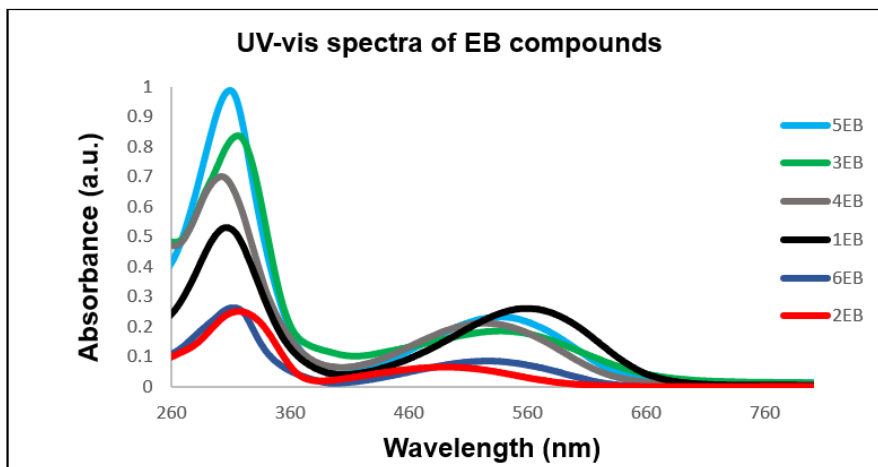


Figure 19. UV-vis spectra of TANI-EB compounds (1-6).

The UV-vis spectra of 1EB, 3EB, and 4EB compounds reveal that they do not differ substantially in $\lambda_{1\max}$ values and are in excellent agreement with the previously synthesized compounds in Faul's group in terms of molecular structure and oxidation state.¹ (Table 4).

Table 4. Comparison between λ_{\max} values in the previous study vs. the current study.

Compound	previous study in THF		current study in CHCl ₃	
	$\lambda_{1\max}$	$\lambda_{2\max}$	$\lambda_{1\max}$	$\lambda_{2\max}$
1EB	308 nm	568 nm	307 nm	560 nm
2EB	332 nm	506 nm	317 nm	490 nm
3EB	320 nm	558 nm	316 nm	537 nm
4EB	306 nm	538 nm	302 nm	523 nm

The λ_{\max} values show a hypsochromic effect (blue shift) for all compounds in the current study. The blue shift of these absorption peaks can be attributed to the solvent change. As the spectrum is measured in different solvents, the location and intensity of the absorption peaks can vary. Due to the hydrogen bonding in THF, we have more interaction compared to CHCl₃ which leads to larger λ_{\max} values than in the previous studies.

Reference

- 1) Faul, C. F. J. Chem. Eur. J. 17, **2011**,12512 – 12521.

CHAPTER IV. Crystallization

Crystallization is the arrangements of molecules into a three-dimensional ordered structure and is governed by the fundamental laws of thermodynamics and kinetics. The primary key factor that plays a decisive role in solution-based crystallization is supersaturation, where the solution concentration is greater than the product solubility.

Nucleation and crystal growth are two of the main steps of the crystallization process. In the nucleation step, dissolved molecules in the supersaturated solution start to aggregate, giving rise to the growth of nuclei, serving as sites with low surface energy for crystallization to occur. It should be noted that the diffusion and incorporation of particles onto the surface of the established nuclei and their integration into the crystal lattice controls the growth stage in crystal formation.

IV.1. Nucleation

The fundamental complexity of the nucleation process and providing a clear definition of the mechanism derives from the fact that the critical nucleus sizes usually come within the range of 10-1000 molecules, which are rarely accessible for most of the current studies.¹ In fact, they simply migrate across the determined volume of solution and at the same time live for very brief periods that drastically minimize the appearance changes in the volume of the initial solution.²⁻³

Owing to its theoretical simplicity, the classical nucleation theory (CNT) explanation of the nucleation mechanism is the most commonly adapted theory. This theory evolved in the early 20th century from the studies of Gibbs and many other scientists; it was initially developed for the condensation of vapor into a liquid. The free energy diagram for nucleation is shown in Figure 20.

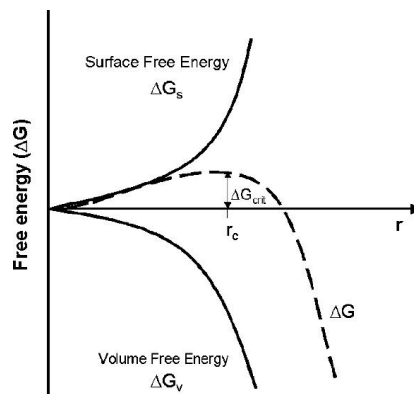


Figure 20. Free energy change diagram of forming a nucleus.²

This graph shows a relationship between the free energy change needed for the nucleation (ΔG) vs. the nucleus radius (r). The mathematical representation of this graph is shown in Equation 1.¹

$$\Delta G = \frac{-4\pi r^3}{3\vartheta} k_B T \ln S + 4\pi r^2 \sigma \quad \text{Eq.1}$$

where:

ΔG = change in free energy of the system

r = nucleus radius

ϑ = volume of single molecule

k_B = Boltzmann's constant

T = absolute temperature

S = vapor supersaturation ratio

σ = specific surface energy

This equation can be simplified to:

$$\Delta G = \Delta G_v + \Delta G_s$$

Based on this equation, the total free energy (ΔG) corresponds to the difference in the volumetric change of free energy required for the phase transformation (ΔG_v) and the surface formation (ΔG_s). When the whole term (ΔG) is less than zero, transformation takes place. As we convert this thermodynamic definition to the crystallization process, the first expression reflects the intrinsic propensity of the supersaturated solution to deposit.

For crystal precipitation, from a supersaturated solution, the free energy reduction in the phase transformation is due to the fact that the solid-state is thermodynamically more stable than the liquid state and thus the (ΔG_v) is negative. This reduction in ΔG_v favors nucleus growth. The surface energy rise in the second term can be attributed to the formation of the phase boundary with a surface area equal to $4\pi r^2$ and surface energy (σ) at the nucleus surface which predominates for small r . This implies that the nucleation is a competition between ΔG_v and ΔG_s , where the winner determines the overall sign of ΔG .

For the nucleus to reach maximum free energy, a critical size with radius (r_c) is required (Figure 20). Beyond this maximum point, the energy you spend creating new surfaces is relatively small compared to the energy you get from transformation and as a consequence, the crystal embryo will grow and crystal nuclei arrange themselves in a lattice. Below this point, the cluster will shrink.

Differentiate Equation 1 with respect to r yielding the r_c in Equation 2.¹

$$r_c = \frac{2\sigma}{k_B T \ln S} \quad \text{Eq.2}$$

The energy associated with this critical radius is the activation energy and is a barrier resisting the cluster growth. It is represented by Equation 3.¹

$$\Delta G_{\text{crit}} = \frac{16 \pi \sigma^3 \vartheta^2}{3 k_B^2 T^2 \ln S^2} \cdot f(\theta) \quad \text{Eq.3}$$

Where:

σ = specific surface energy
 ϑ = volume of single molecule
 k_B = Boltzmann's constant
 T = absolute temperature
 S = vapor supersaturation ratio
 $f(\theta)$ = geometric factor

Vapor supersaturation ratio (S) is the ratio of vapor pressure to the pressure of saturated vapor. Geometric factor ($f(\theta)$) used for heterogeneous nucleation and can be defined in Equation 4.

$$f(\theta) = (2 + \cos \theta) (1 - \cos \theta)^2 / 4 \quad \text{Eq.4}$$

Where:

θ = contact angle

Equation 5 can be used to determine the nucleation rate.⁴

$$I = I_0 \exp\left[-\frac{16\pi}{3} \frac{\gamma_{sl}^3}{(\rho \Delta s_f \Delta T)^2 k_B T} \cdot f(\theta)\right] \quad \text{Eq.5}$$

where:

I_0 = nucleation rate
 γ_{sl}^3 = surface energy between solid and liquid
 ρ = density
 Δs_f = specific entropy of fusion of species
 ΔT = total undercooling
 k_B = Boltzmann's constant
 T = absolute temperature
 $f(\theta)$ = geometric factor

The I_0 is a prefactor that contains atomic vibration frequency, probability of capturing an atom at the surface, and the number density of the nuclei in the liquid.

On the basis of this equation, the temperature dependence of growth rate is dominated by two competing terms in the denominator of exponential Equation 4. Increasing undercooling has a large impact on ΔT^2 term which results in decreasing the nucleation barrier and as a consequence increasing the nucleation rate. On the other hand, the nucleation rate is reduced by lowering the atomic movement at lower temperatures (T).

IV.2. Homogenous and heterogeneous nucleation

Nucleation can occur in two ways, either homogeneously or heterogeneously.⁵ Homogeneous nucleation is identified without favored nucleation sites and happens in any part of the system. The lack of a microstructure can lead to homogenous nucleation in gases, while heterogeneous nucleation at the surfaces is inevitable.

Equation 2 explicitly relates the critical radius size to surface energy. Often, the critical radius size is too large for a nucleus to precipitate out and as a consequence, the nuclei with this critical size have much more surface energy than typical impurity atoms. Based on the Boltzmann equation, the probability of producing such a high energy nucleus with a substantial critical size is low. This implies that the homogeneous nucleation is less likely to occur in the liquid-solid transformation.

While the homogeneous nucleation model has been effective in addressing some aspects of nucleation kinetics in more compact structures, studies show the "heterogeneity" of nucleation in these systems.⁶

Heterogeneous nucleation occurs on foreign bodies and is effectively facilitated by impurities. Phase change transformation in heterogeneous nucleation has a significantly lower energy barrier than homogeneous nucleation and is more dominant.⁵ A schematic representation for heterogeneous nucleation is demonstrated in Figure 21.

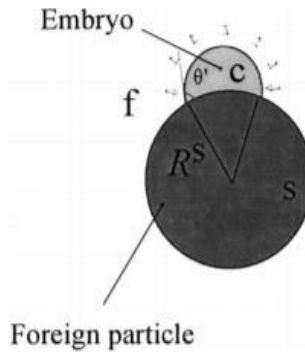


Figure 21. The heterogeneous nucleation of a spherical solid cap at a foreign particle.⁵

Unlike homogeneous nucleation, heterogeneous nucleation interacts firmly at the foreign surface and has a good structural match with the nucleating phase.⁵ A combination of the three surface energies between the solid, liquid, and foreign surfaces defines how the wetting angle (θ) is measured.

IV.3. Classical nucleation theory (CNT)

The basis of CNT is built on the number of assumptions to explain the nucleation process in a simple way which results in limitations.² Most fundamentally, this theory assumed the nucleus as a droplet model with a defined shape and assigned the same macroscopic properties of the bulk phase to the droplet. The consequence of this statement is that the molecular configuration in the initial steps of the crystal formation is the same as in a grown crystal. Besides, the critical nuclei sizes, the interface between vapor–liquid is treated as planar.¹ According to the capillary approximation for the planar interface between vapor–liquid, large nuclei can be suitable for this purpose, although, for small nuclei with sharply angled surfaces, the theory leads to major differences. Growth development is restricted to the consecutive introduction of a building block (molecule) to the cluster and the possibility of collision between more than two particles or collision between pre-existing clusters are overlooked. A schematic representation for CNT is demonstrated in Figure 22.

Although the CNT is sufficiently helpful to understand the fundamental dynamics of the phenomena and have a strong qualitative analysis on nucleation data, its inability to provide an accurate and adequate quantitative explanation limits the use of CNT for a variety of systems.

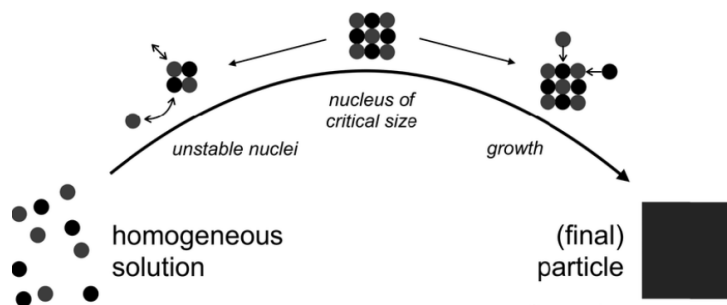


Figure 22. Schematic illustration for CNT.⁷

IV.4. Two-step nucleation theory

Recently, the two-step nucleation of crystals has emerged as a major research interest. This theory allows us to explain certain questions which in the classical nucleation explanation were not resolved. Questions like the incompatibility in CNT nucleation rates value and theoretical predictions, the function of heterogeneous components for polymorph selection, the function of stable and unstable phases, and many other questions.⁸ Computational simulations were performed by ten Wolde and Frenkel to provide insights into the two-step mechanism.^{8a} In parallel to computational studies, the theoretical investigations have also shown the nucleation through a two-step nucleation mechanism.² Based on this theory, the nucleation does not occur through the supersaturated old stage by inserting building blocks one by one to extend the crystal lattice and form an embryonic nucleus, where proposed in classical nucleation theory but takes rather more complicated routes.⁹

Two-step nucleation theory was first discovered in proteins.¹⁰ The schematic illustration of this mechanism is shown in Figure 23. According to this non-classical nucleation theory, the first stage consists of the creation of a cluster with adequate size which occurs within mesoscopic clusters of dense liquid (Figure 23).² The existence of the amorphous metastable clusters in the homogeneous solutions before nucleation plays a significant role in the efficiency of this model.⁸ In the next step, formed clusters morph into a well-defined shape. The formation of the organized cluster is the slowest and therefore the rate-determining step, which aligns with the fact that as the conformational flexibility of the growing crystal increases, the growing crystal needs more time to arrange itself into the long-range ordered structures.² It should be noted that the existence of the amorphous metastable clusters in the homogeneous solutions before nucleation plays a significant role in the efficiency of this model.^{8,9}

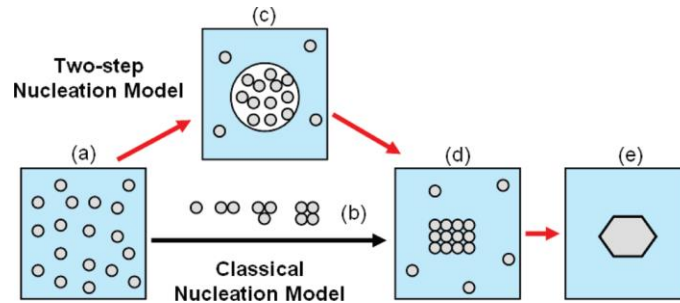


Figure 23. Schematic representation of nucleation theories: (a) supersaturated solution; (b) ordered subcritical cluster of solute molecules, (c) liquid-like cluster of solute molecules, (d) ordered crystalline nuclei; (e) solid.²

IV.5. The Morphology and growth of crystals

After nucleation, the crystal shape is affected by two factors: a) Anisotropy of surface energy b) Growth kinetics.

IV.5.1 Wulff construction of surface energy

In general, the surface free energy of the crystal depends on the particular crystallographic planes that make up its surface. The favored planes are those that minimize overall surface energy.¹¹ Wulff construction is an essential model for describing and predicting the equilibrium morphology of the particles given the surface energies of the material in the thermodynamic system.^{12,13} Surface free energy minimization is used to explain the advantages of certain crystal planes over others. Equation 6 illustrates the surface energy of the particle.¹⁴

$$G = \sum_i \gamma_i A_i \quad \text{Eq.6}$$

where:

γ_i = surface energies of each type of facets

A_i = surface areas for each type of facets

Surface free energy minimization determines the equilibrium shape of the crystal in Equation 7.

$$\int \gamma_i dA = \text{minimum} \quad \text{Eq.7}$$

The Wulff construction should be applied to determine the crystal shape when structural anisotropy exists. Structural anisotropy, and therefore physical

property anisotropy, arises when there is direction-dependent variation in atomic bonding within a crystal.

Graphic illustration of Wulff construction (γ – plot) is shown in Figure 24.

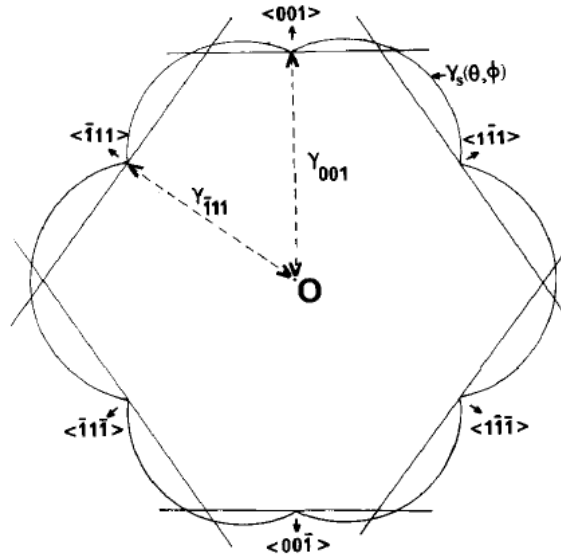


Figure 24. Wulff plot scheme.¹⁵

The equilibrium shape of a crystal is the inner envelope shape enclosed in the actual shape. Surface free energy can be determined by drawing a perpendicular distance from the origin (O) to each face of the crystal. The distance between the origin and the face (dashed line) is proportional to surface free energy ($\gamma_s(\theta, \Phi)$). Surface energy is defined in polar spherical coordinates where θ is the angle from the polar direction to the plane normal and Φ is the azimuthal angle.

IV.6. Growth kinetics

Usually, a crystal develops in a non-equilibrium condition and its final shape is determined by several factors that contribute to growth kinetics.¹⁶ Major steps that can be considered as crystal growth in the solution are governed by a) the transport of the solute to the surface of the crystal from the bulk and b) surface integration.

Kossel's model is typically used in the surface analysis to determine macroscopic surface characteristics. Figure 25 demonstrates the face profile in Kossel's model. For simplicity, atoms are substituted by cubes and can either adsorb on the surface or the step sites. The same scenario applies to the

incorporation site.¹⁷This approach is a simple representation of crystal surface for atomic crystallization. however, it is a very useful approximation that we can use to understand the molecular crystallization.

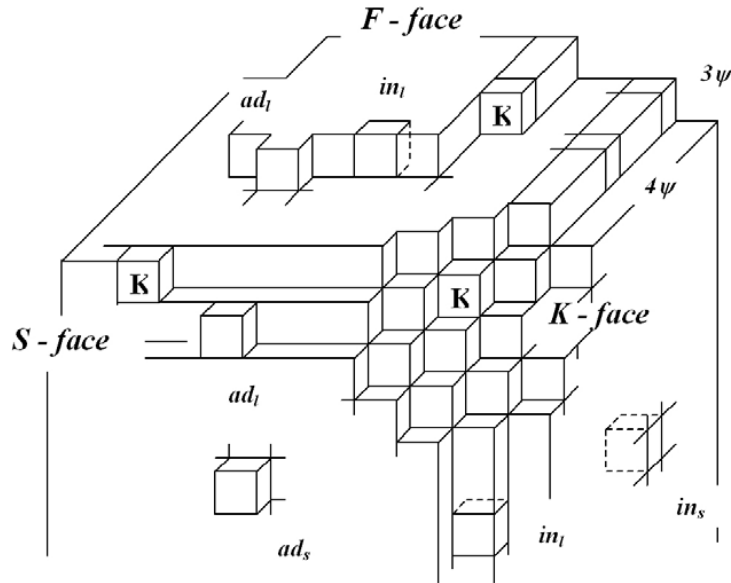


Figure 25. The face profile in Kossel's model.¹⁷

The adsorption and incorporation sites' bonding energies compete with each other and are equal to the binding energy at the kink (kink is the only site that exists in thermodynamic equilibrium). This relationship is illustrated in Equation 8.

$$\varphi_{ad} + \varphi_{in} = 2\varphi_{kink} \quad \text{Eq.8}$$

The kink term (φ_{kink}) consists of two parts. The first is the attachment energy known as the released energy per mole of molecules for a newly formed layer on the crystal surface. The growth rate is directly proportional to attachment energy. The second is the slice energy (the interaction with half of a building block's nearest neighbors)¹⁷

Attachment energy determines the crystal shape and it is characterized by a Wulff plot where the distance between the origin and the face corresponds to the amount of attachment energy.¹⁸

The concept behind the discussed theory can be applied to optimize the techniques for growing crystals. Since nucleation occurs homogeneously in this study (all crystals grow in the bulk, not on the substrate) all samples were filtered

through a syringe filter to avoid external particles (dust) being introduced into the vial.

IV.7. Different techniques for growing single crystal

The functionality and efficiency of organic electronic devices are shown to be dictated by the solid-state morphology of conjugated polymers.¹⁹ Single-crystal provides an opportunity to understand the inter- and intramolecular interactions in the crystal structure.

Crystallization is one of the oldest purification techniques and in most cases growing a single crystal is an art, and patience is the key throughout the process. Common crystallization techniques to grow organic single crystals include slow evaporation, slow cooling, vapor diffusion, liquid-liquid diffusion, and so on.

The vapor diffusion and liquid-liquid diffusion techniques use as a crystallization technique for small molecules and by far are the best methods to use. In both techniques, we need to find a suitable solvent for the sample. This can be accomplished by bringing the sample into the desired concentration.

Liquid-liquid diffusion technique or layering involves the slow diffusion of one solvent into another. In the binary solvent system, the first solvent dissolves the compound, and the second solvent precipitates the solid out of the supersaturated solution. Special care is needed while transferring the second solvent on top of the first solvent. Over time the second solvent diffuses into the first solvent and the solubility decreases gradually, inducing supersaturation, leading to crystallization. The set-up for the liquid-liquid diffusion technique is shown in Figure 26.

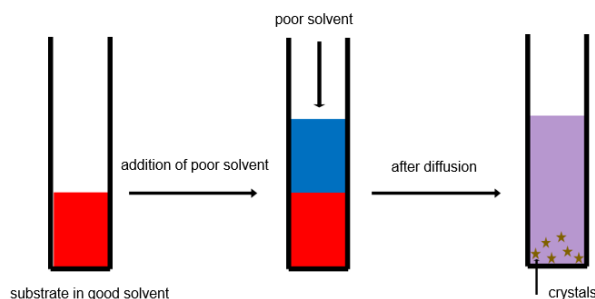


Figure 26. A typical liquid-liquid diffusion setup used in growing crystal

Crystallization by vapor diffusion is most frequently done by choosing a solvent in which the compound is insoluble and is more volatile than the

saturated solution. The crystal growth by the vapor diffusion method is typically performed in closed or semiclosed systems. Over time, the volatile solvent diffuses into a suitable container inside the sealed vial, which causes a decrease in solubility and therefore, facilitating the crystal growth. The vapor diffusion setup is illustrated in Figure 27.

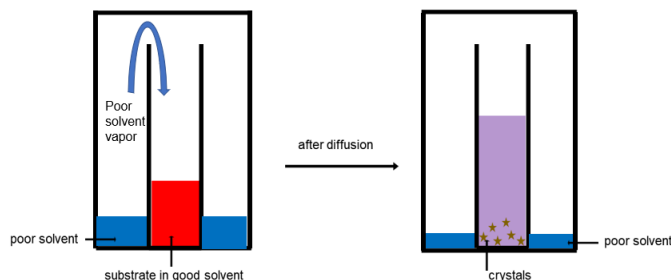


Figure 27. A typical vapor diffusion setup used in growing crystal

IV.8. Vapor diffusion results

In this study, single crystals of 4EB, 5EB, and 6EB were grown at room temperature in the bulk using the vapor diffusion method. Once crystals grew they were moved onto the silicon wafer (silicon wafer were used as a smooth surface to make crystal structure analysis easy in future). The first essential step for crystallization is the proper choice of solvent systems. From the solubility results, a series of vapor diffusion crystallization was set up. Due to the non-volatile nature of the solvents (water as the vapor phase), the growth process was long but should give slow crystallization. Glass scintillation vials were selected as the crystal growth containers. All samples were filtered through a syringe filter before transferring into the vial. To prepare the solutions, 1 mg of each compound was dissolved in 1 ml of the desired solvent. Since the 2EB, 4EB, 5EB, and 6EB compounds were soluble in different solvents, they were crystallized under different conditions. The results are presented in Figure 28. Optical microscope images were collected at room temperature. We did crystallization in the bulk and then crystals moved onto the silicon wafer. We used reflection on the silicon wafer with a cross-polarized filter to produce the contrast.

The best solvent systems were found to be DMF: H₂O for 2EB and 4EB and DMSO: H₂O for 5EB and 6EB. Single crystals of 2EB, 4EB, 5EB, and 6EB have lengths of approximately 107 μm , 239 μm , 98 μm , and 352 μm ,

respectively. The height of 4EB and 6EB crystals determined by profilometry was approximately 9.1 μm , and 3.42 μm , respectively.

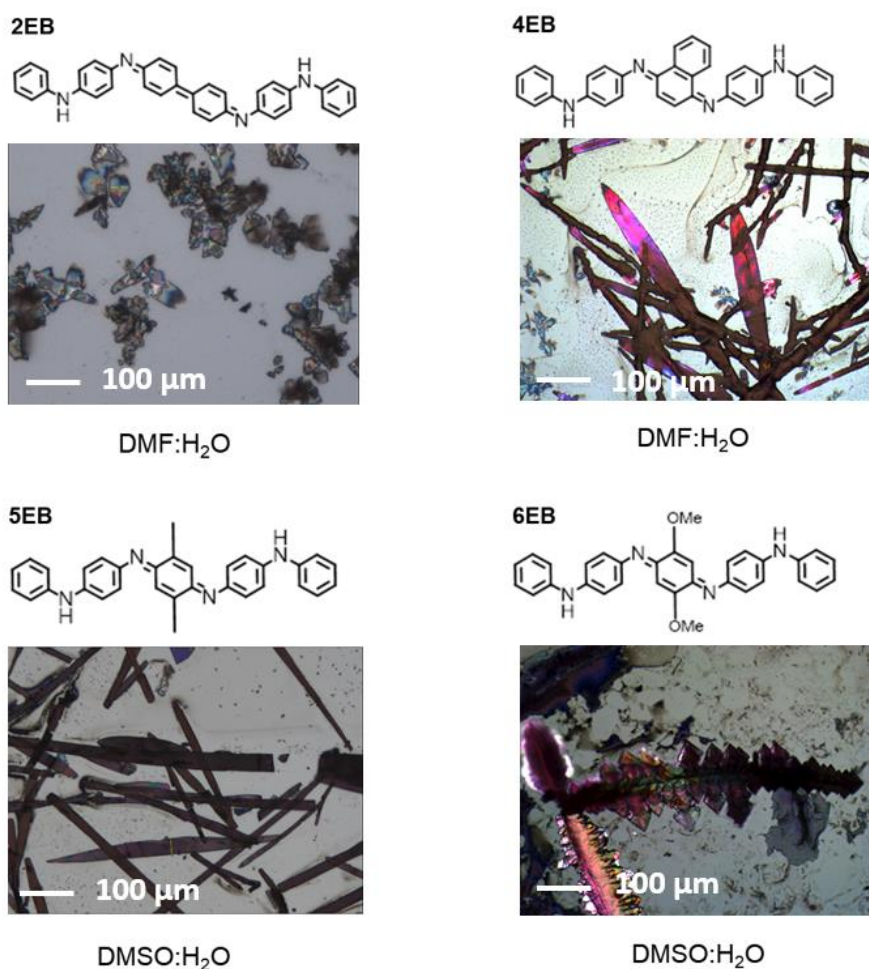


Figure 28. Single crystals of various TANI oligomers in EB oxidation state.

IV.9. Layering results

From the solubility results, a series of liquid-liquid diffusion setups were prepared. Glass vials were selected as the crystal growth containers. All samples were prepared at room temperature and filtered through a syringe filter before transferring into the vial. To prepare the solution, 1 mg of each compound was dissolved in 1 ml of the desired solvent. The best results were obtained from $(\text{CH}_3)_2\text{CO}:\text{H}_2\text{O}$, $\text{CH}_3\text{CN}:\text{H}_2\text{O}$, and $\text{THF}:\text{H}_2\text{O}$ for the 4EB compound (Figure 29). $\text{DMF}:\text{H}_2\text{O}$, $\text{NMP}:\text{H}_2\text{O}$, and $\text{THF}:\text{H}_2\text{O}$ were found to be good solvent systems for the 6EB compound (Figure 29). Optical microscope images were collected at room temperature. We did crystallization in the bulk and then crystals moved

onto the glass slide. We used transmission on the glass slide with a cross-polarized filter to produce the contrast.

Based on the above discussion, both layering and vapor diffusion can yield good crystals for X-ray diffraction and possibly mechanical and electrical analysis. It is found that only a few combinations of the solvent systems produced high-quality single crystals. Of the 4 compounds used for crystallization, 2 compounds (4EB and 6EB) produced large enough single crystals for the determination of X-ray structure.

One of the major challenges was the creation of high-quality single crystals for compounds 1EB due to the presence of two inseparable isomeric structures in the solid-state. Producing high-quality single crystals for compounds 3EB is currently under investigation.

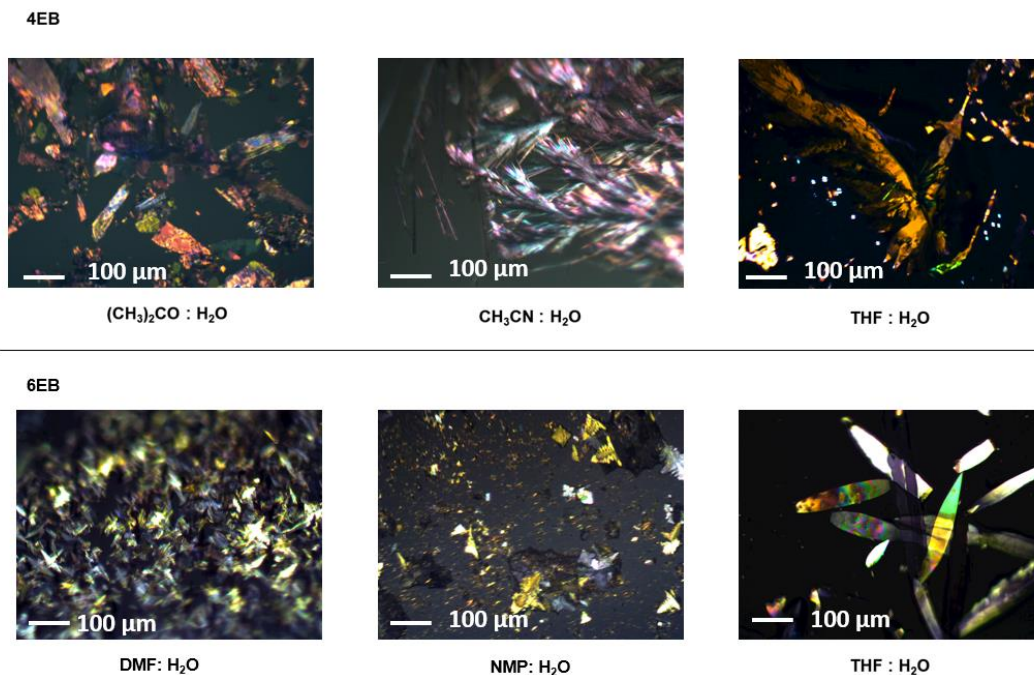


Figure 29. Different solvent systems used for single crystal growth for 4EB and 6EB.

References

- 1) Karthika, S. Kalaichelvi, P. Cryst. Growth Des. 16, **2016**, 6663–6681.
- 2) Erdemir, D. Lee, A, Myerson. A. Acc. Chem. 42, **2009**, 621-629.
- 3) Schuth, F. Bussian, P. Agren, P. Linden, M. Solid State Sci. 3, **2001**, 801–808.
- 4) Shibuta, Y. Sakane, S. Ohno, M. Acta Mater. 105, **2016**, 328-337
- 5) Liu, X. Y. J. Chem. Phys. 112, **2000**, 9949-9955.
- 6) Turnbull, D. J. Chem. Phys. 18, **1950**, 198- 203.
- 7) Gebauer, D. Raiteri, P. Gale, J. D. Cölfen, H. Am. J. Sci. 318, **2018**, 969-988.
- 8) Vekilov, P. G. Nanoscale. 2, **2010**, 2346–2357. 8a) ten Wolde, P. R. Frenkel, D. Science, **277**, 1997, 1975–1978.
- 9) Ito, F. Suzuki, Y. Fujimori, J, Chapelle, M. L. Sci. Rep. 6, **2016**, 22918.
- 10) Lutsko, J. F. Sci. Adv. 5, **2019**, 1-8.
- 11) Ringe, E. Van Duyne, R. P. Marks, L. D. Nano Lett. 11, **2011**, 3399–3403.
- 12) Guisbiers, G. José-Yacaman, M. Use of Chemical Functionalities to Control Stability of Nanoparticles, Elsevier, **2017**.
- 13) Wolf, D. E. J. Phys. A: Math. Gen. 20, **1987**, 1251-1258.
- 14) Yu, Z. Flodström, A. Surf. Sci. 401, **1998**, 236–247.
- 15) Marks, L. D. J. Cryst. Growth. 61, **1983**, 556—566.
- 16) Dobrushin, R. L. Kotecký, R. Shlosman, S. B. Wulff construction: a global shape from local interactions. AMS Translation Series, Providence, chapter 1, 1992.

- 17) Aquilano, D. Abbona, F. Morphology of Crystals Grown from Solutions, Springer Handbook of Crystal Growth, Springer, 2014.
- 18) Coombes, D. S. Catlow C. R. A. Price, S. L. Cryst. Growth. Des. 5, **2005**, 876- 885.
- 19) Curtis, M. D. Cao, J. Kampf, J. W. JACS, 126, **2004**, 4318-4328.

Chapter V. Conclusion

By utilizing the Buchwald-Hartwig coupling reaction we synthesized different tetraaniline oligomers varying in central aromatic core and characterized them using

$^1\text{H-NMR}$ and UV-vis spectroscopy. UV-vis measurements proved that 1EB, 2EB, 3EB, and 4EB compounds were structurally identical to the emeraldine state form. The currently available $^1\text{H-NMR}$ and UV-vis spectra for compound 1EB suggest that this compound exists in a mixture of isomers.

Time-quenched experiments for the LE-to-EB oxidative reaction using APS for compounds 2EB and 3EB revealed that the conversion to EB significantly slowed down after 1 minute while a maroon insoluble solid was formed, which suggests that the oxidation reaction has a tendency to over-oxidize to the pernigraniline form. Results from the oxidation of LE to EB base using Ag_2O instead of APS for compounds 1EB, 2EB, and 3EB suggest that oxidation by APS is more efficient than Ag_2O and compounds 2EB, and 3EB are oxidized more easily by APS than Ag_2O . No significant difference was observed for the 1EB compound. To investigate how the change in APS equivalent affect yield we changed APS equivalent from 1 eq to 1.5 and 2 eq for compounds 2EB and 3EB while keeping other variables constant during the experiment. We observed that a higher conversion rate was obtained when 1 eq of APS was used.

The UV-vis spectra of 1EB, 3EB, and 4EB compounds revealed that they do not differ substantially in $\lambda_{1\text{max}}$ values and are in excellent agreement with the previously synthesized compounds in Faul's group in terms of molecular structure and oxidation state. Also, UV-vis spectra of compounds 4EB, 5EB, and 6EB confirmed that they are in the emeraldine oxidation state with characteristic absorption maxima at 523, 538, and 526 nm respectively. The presence of the second peak ($\lambda_{2\text{max}}$) unambiguously indicates that all these compounds are in their emeraldine base form. The UV-vis analysis of the 5LE compound in chloroform produced confusing results. In chloroform, it appears that the 5LE also contains some of the 5EB, but NMR opposes this fact.

Single crystals of 2EB, 4EB, 5EB, and 6EB were grown at room temperature using the vapor diffusion method. The best solvent systems were found to be

DMF: H_2O for 2EB and 4EB and DMSO: H_2O for 5EB and 6EB compounds. Single crystal of compounds 2EB, 4EB, 5EB, and 6EB having a length of approximately 107 μm , 239 μm , 98 μm , and 352 μm , respectively. The height of 4EB and 6EB crystals were determined by the profilometry technique and assigned to be 9.1 μm , and 3.42 μm , respectively. Single crystals of 4EB and 6EB were obtained by the layering technique. DMF: H_2O , NMP: H_2O , and THF: H_2O were found to be good solvent systems for 6EB and $(\text{CH}_3)_2\text{CO}$: H_2O ,

CH₃CN: H₂O, and THF: H₂O were found to be appropriate solvent systems for 4EB.

One of the major challenges was the failure to produce high-quality single crystals for compounds 1EB due to the presence of two isomeric structures in the solid-state. Producing high-quality single crystals for compounds 3EB is under investigation.

Our long-term approach is to study the structure-property relationships of these oligoaniline single crystals by solving the crystallographic packing and carrying out the mechanical and electrical property measurements of these single crystals. Once fully characterized, these oligomer crystals with different morphologies can serve as the crystalline filler materials in the disordered polyaniline matrix to create bio-inspired composites.